EurJIC
European Journal of Inorganic Chemistry

A Journal of ChemPubSoc Europe

Accepted Article

Title: Synthesis, Characterization, and Magnetic Properties of a Series of Copper(II) Chloride Complexes of Pyridyliminebenzoic Acids

Authors: Elena Buvaylo, Vladimir Kokozay, Valeriya Makhankova, Andrii Melnyk, Maria Korabik, Maciej Witwicki, Brian Skelton, and Olga Vassilyeva

To be cited as: *Eur. J. Inorg. Chem.* 10.1002/ejic.201701391

Link to VoR: http://dx.doi.org/10.1002/ejic.201701391

WILEY-VCH

10.1002/ejic.201701391

WILEY-VCH

Synthesis, Characterization, and Magnetic Properties of a Series of Copper(II) Chloride Complexes of Pyridyliminebenzoic Acids

Elena A. Buvaylo,[a] Vladimir N. Kokozay,[a] Valeriya G. Makhankova,[a] Andrii K. Melnyk,[b] Maria Korabik,[c] Maciej Witwicki,[c] Brian W. Skelton,[d] and Olga Yu. Vassilyeva*[a]

Dedicated to Professor Julia Jezierska in honour of her seventieth anniversary

Abstract: A series of Cu(II) halide complexes, $Cu(HL1)Cl_2·CH_3OH$ (**1**), $[Cu(L1)Cl]_2·H_2O$ (**2**), $[Cu(HL2)Cl_2]_2·2DMF$ (**3**), $[Cu(HL2)_2Cl]_nCl_n·2nH_2O$ (**4**) and $[Cu(L3)Cl]_n$ (**5**), containing pyridyliminebenzoic acids HL1, HL2 and HL3 derived from *o*-, *m*- and *p*-aminobenzoic acids, respectively, have been obtained as single crystals and characterized by elemental analysis, IR, EPR spectroscopy, magnetic measurements and single-crystal X-ray diffraction techniques. The results obtained show the formation of molecular (**1**), dimeric (**2**, **3**) and polymeric structures (**4**, **5**) based on chloride (**1–4**) and carboxylate bridges (**5**) with copper(II) atoms in the square-pyramidal geometry of varying degrees of distortion. In the case of **2** and **5** the ligand deprotonation was completely achieved even in the absence of a base. The closest Cu···Cu separations are found in the crystal lattices of the polymer **5** (3.33 Å) and dimers **2** (3.35 Å) and **3** (3.38 Å). The X-band polycrystalline EPR spectra of **1–3** with typical axial patterns show no indication of exchange interactions between copper ions in the range 295–77 K. The observed rhombic features of the EPR spectra of **4** arise from the coupling of g-tensors from differently oriented Cu(II) coordination polyhedra in the solid state. A characteristic spin-triplet EPR spectrum of **5** at 77 K was simulated using the spin-Hamiltonian parameters for $S = 1$, $g_x = 2.08$, $g_y = 2.11$, $g_z = 2.37$ and the value of the zero-field splitting parameter D of 0.137 cm^{-1}. Magnetic susceptibility measurements revealed antiferromagnetic (**1–3**, **5**) and ferromagnetic coupling (**4**) between the metal atoms at low temperatures. Theoretical methods were employed to provide additional insight into magnetic interactions in the studied compounds.

Introduction

Alpha-iminopyridine Schiff base ligands whose nitrogen atoms are perfectly placed to act cooperatively in cation binding are electronically similar to classic bipyridines. Metal complexes of the latter have shown remarkable properties in photochemistry, photophysics, electrochemistry, supramolecular chemistry, molecular devices and machines.[1] However, substitution reactions at the bipyridine backbone to tune the desired properties of the resulting complexes are challenging from a synthetic viewpoint and α-iminopyridines serve an attractive alternative in this respect. A facile preparation of α-iminopyridines by simple condensation between 2-pyridinecarbaldehyde (2-PCA) and primary amine have afforded a number of metal complexes that were screened for catalytic, luminescent, photophysical, electrochemical and magnetic properties.[2–5] Nevertheless, iminopyridine compounds remain less explored than bipyridine complexes.

Alpha-iminopyridines bearing free carboxylate ends are considered highly useful due to their simultaneous activities as both chelator and a bridging ligand adopting various coordination modes. Aromatic amino acids have proven themselves very efficient in the design of carboxylate incorporated Schiff base ligands.[6]

Metal complexes with halide bridges have been structurally and magnetically characterized in detail. Over the past several decades, interest in low-dimensional Cu(II) molecular magnetic systems in which superexchange pathways involve diamagnetic halide ions has had a revival in large part owing to the advent of high-temperature superconductors.[7] As the structural variety is very large, the metal atoms show a wide range of values for the coupling constant. As a result, the magnetostructural correlations for halide-bridged Cu(II) dimers and polymers are less obvious than those for hydroxo- and alkoxo bridged copper compounds. DFT calculations have proven to be a powerful tool when applied to the field of molecular magnetism. Theoretical methods can provide significant support for magnetic-exchange pathways developed from experimental data.[8]

We have been exploring the chemistry of the Schiff-base ligands that originate from the condensation of 2-PCA and amino benzoic acids towards 3d metals (Cr, Mn, Co, Ni, Zn) with the aim of producing novel complexes with diverse potential advantages.[9] We have now extended our investigations to copper and describe herein the formation and crystal structures of five new copper(II) complexes, $Cu(HL1)Cl_2·CH_3OH$ (**1**), $[Cu(L1)Cl]_2·H_2O$ (**2**), $[Cu(HL2)Cl_2]_2·2DMF$ (**3**), $[Cu(HL2)_2Cl]_nCl_n·2nH_2O$ (**4**) and $[Cu(L3)Cl]_n$ (**5**), containing pyridyliminebenzoic acids HL1, HL2 and HL3 derived from *o*-, *m*- and *p*-aminobenzoic acids, respectively (Scheme 1, DMF – N,N-dimethylformamide). The position of the carboxylate group in the structural isomers HL1–HL3 influences the amount of chloride ligands in the coordination environments around the copper atoms in **1–5** what imposes the particular bridging pattern between metal centers. Magnetic susceptibility measurements revealed antiferromagnetic (**1–3**, **5**) and ferromagnetic coupling (**4**) between the Cu atoms. The data obtained were compared to the exchange parameters of other Cu(II) dimers and polymers

[a] Department of Chemistry, Taras Shevchenko National University of Kyiv,
64/13 Volodymyrska str., Kyiv 01601, Ukraine.
Phone +380 44 235 4371
E-mail: vassilyeva@univ.kiev.ua
www.chem.univ.kiev.ua
[b] Institute for sorption and problems of endoecology, the National Academy of Sciences of Ukraine,
13 Generala Naumova str., Kyiv 03164, Ukraine
[c] Faculty of Chemistry, University of Wroclaw,
F. Joliot-Curie 14, Wroclaw 50-383, Poland
[d] School of Molecular Sciences, M310, University of Western Australia, Perth, WA 6009, Australia

Supporting information for this article is given via a link at the end of the document.

with chloro bridges to assess their consistency with known magnetostructural *J*-correlations. Moreover, theoretical methods were employed to provide a detailed analysis of the electronic structures of the complexes and independent evaluation of the magnetic coupling constants.

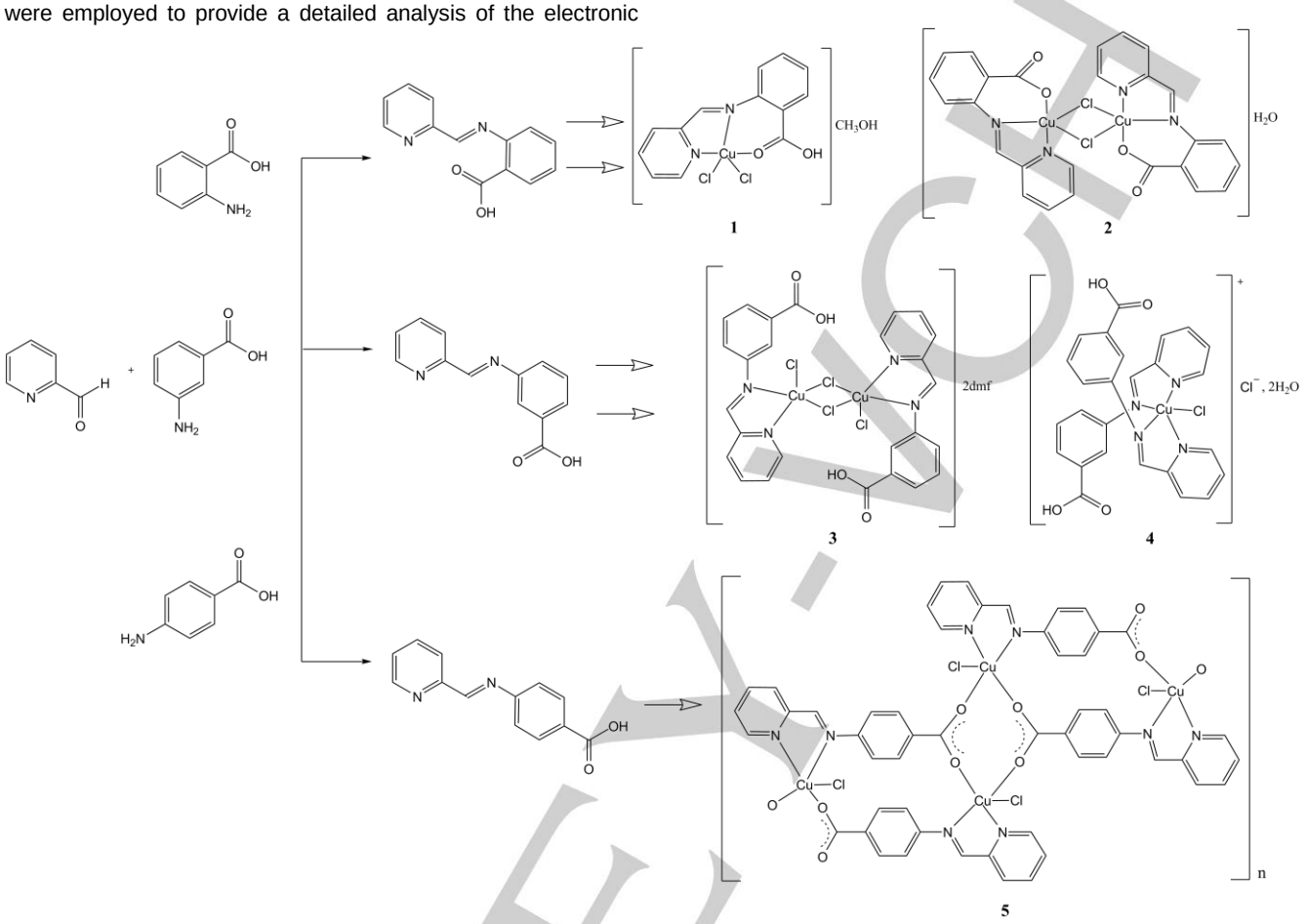

Scheme 1. Formation of Schiff base ligands HL1, HL2 and HL3 and respective copper(II) complexes **1**–**5**.

Results and Discussion

Synthesis and IR spectroscopy

Novel Cu(II) chloride complexes **1**–**5** were synthesized from the reactions of the pre-formed Schiff base ligands and $CuCl_2 \cdot 2H_2O$ in methanol or a methanol/DMF mixture and isolated by the solution evaporation method at room temperature.

Compounds with neutral (**1**, **3** and **4**) and deprotonated (**2**, **5**) Schiff base ligands can be easily distinguished based on their infrared spectra (Figs S1–S5). The spectra of **1**, **3** and **4** are dominated by sharp absorptions at 1654 (**1**), 1692 (**3**) and 1708 cm^{-1} (**4**), which are attributed to a C=O stretching vibration of the carboxylic groups. Two strong bands observed at 1596, 1351 (**2**) and 1594, 1392 cm^{-1} (**5**) are due to ν_{as}(COO) and ν_{s}(COO) vibrations of the metal coordinated carboxylate functionalities of HL1 and HL3, respectively. The coordination mode of the carboxylate can be assigned on the basis of the difference of these two frequencies [$\Delta\nu$ = 245 (**2**); 202 (**5**) cm^{-1}], which indicates the presence of monodentate and bridging coordination for **2** and **5**, respectively.[10] Medium intensity bands that appear at 1614 (**1**), 1624 (**2**), and 1598 cm^{-1} (**3**, **4**) are attributed to the imine bonds of HL1 and HL2, respectively. In the case of **5**, the characteristic ν(C=N) absorptions of HL3 merged into the higher energy COO^{-} band. Broad bands observed in the O–H stretching region (3600–3400 cm^{-1}) of the spectra of **1**–**5** with relatively sharp maxima at 3502 and 3428 (**1**), 3524 and 3447 (**2**), 3412 and 3458 cm^{-1} (**4**) are indicative of the presence of carboxylic acid and alcohol OH functional groups along with lattice and adsorbed water molecules with an extensive network of hydrogen bonds. The sharp multiple absorption bands with medium to high intensity that appear around 1600–1360 cm^{-1} correspond to the ν(CC + CN) stretching of the aromatic rings; ν(CH) and out-of-plane bending (CH) vibrations of the rings are found at 3100–3000 cm^{-1} and 786–773 cm^{-1}, respectively. Several peaks arising below 3000 cm^{-1} on a broad band in the spectra of all complexes are ascribed to CH stretching of the –HC=N– groups of the ligands and alkyl groups of the solvents.

Crystal Structures

Cu(HL1)Cl$_2$·CH$_3$OH (***1***)

The compound crystallizes in the monoclinic space group $P2_1/n$; the asymmetric unit consists of one neutral Cu(HL1)Cl_2 molecule and a solvent molecule of crystallization. The copper coordination sphere, CuN_2Cl_2O, has a five-coordinate structure intermediate between a trigonal bipyramid (chlorine atom Cl2 axial) and a square pyramid (carboxylic oxygen O21 apical) and can be described as a distortion of either (Fig. 1). The angular structural index parameter, $\tau = (\beta - \alpha)/60$, evaluated from the two largest angles ($\alpha < \beta$) in the five-coordinated geometry with the ideal values of 1 for an equilateral bipyramid and 0 for a square pyramid,[11] is equal to 0.42 (Table 1). A distorted square pyramidal description is preferred, however, because it better describes the copper coordination geometry in the related compounds **1**–**5** (Table 1). The Cu–N/O bond lengths in **1** follow a pattern similar to that observed in **2**–**5** and other square-pyramidal copper(II) complexes with the axial bond always being longer than the corresponding basal bonds due to Jahn-Teller distortion of the copper(II) ion.[12] Two basal Cu–Cl bonds in **1** show a traditional bonding distance.

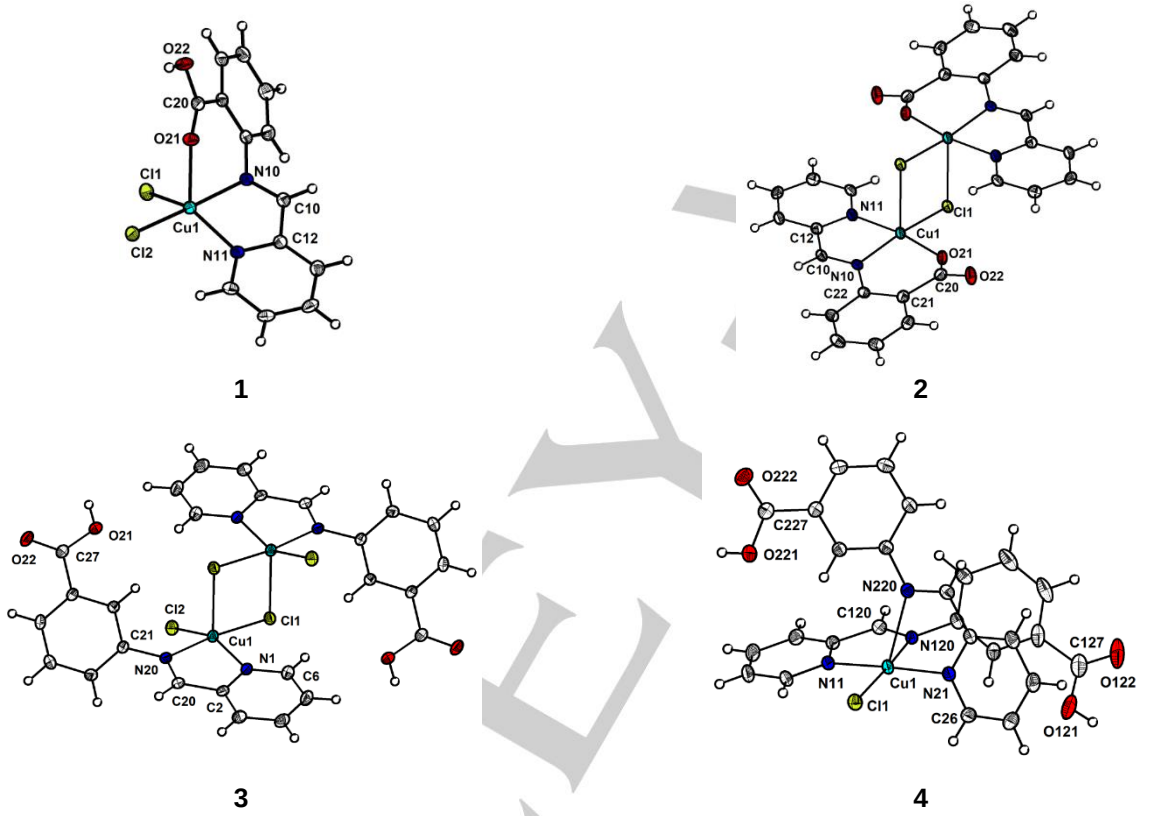

Figure 1. Structures and principal labelling of the molecules of **1–4**. Displacement ellipsoids for non-H atoms are drawn at the 50% probability level. Structure of one of the dimeric molecules is given for **2**.

The lengths of the two carboxylic C–O bonds of 1.225(4) and 1.314(4) Å for **1** unequivocally confirm a molecular form of the Schiff base. The deprotonated tridentate ligand $L1^-$ usually occupies coordination sites in the basal plane of Cu(II) ion forming one five- and one six-membered chelate rings with the metal.[13] With carboxylic oxygen O21 placed at the apical position in **1**, HL1 undergoes considerable strain so that the two fused ring systems are folded along the common Cu(1)−N(10) axis by 52.55°. This greatly distinguishes complex **1** from **2** and other copper compounds of the same Schiff base ligand and different counteranions which show the folding angle of 1.47 (**2**), 14.6 ($F_3CCO_2^-$),[13a] 15.28 (NCS^-),[13b] 23.58 ($C_2O_4^{2-}$),[13c] and 28.60° (NO_3^-, N_3^-).[13a]

There is a hydrogen bond between the OH hydrogen on the carboxylic group to the oxygen atom of the methanol solvent molecule (Table 2). A further, but weaker hydrogen bond, between the methanol OH hydrogen atom and Cl2 of the molecule related by a cell translation along the *c*-axis generates a hydrogen-bonded dimer (Fig. 2). Another chloride atom attached to the metal centre, Cl1, very weekly interacts with a π-system of the neighbouring pyridyl ring with the Cl1···centroid distance of 4.04 Å. The parallel pyridyl rings of the adjacent molecules of **1** also display π···π stacking with the ring centroid distance of 3.54 Å (Fig. 2). The hydrogen bonding, π···Cl and π···π noncovalent interactions afford Cu···Cu separations in the crystal lattice equal to 8.69, 6.34 and 7.65 Å, respectively.

Table 1. Geometrical parameters (bond distances, Å, and angles, °) of the distorted square-pyramidal coordination environment of Cu(II) in **1–5**[a]

	$Cu–X_{basal}$	$Cu–X_{ax}$	*trans* angles at Cu(II)	*cis* angles at Cu(II)
$Cu(HL1)Cl_2·CH_3OH$ (**1**)				
Cu(1)–N(10)	2.005(2)		142.13(7);	79.82(10)–
Cu(1)–N(11)	2.030(2)		167.03(7)	113.85(8)
Cu(1)–Cl(1)	2.2601(8)			
Cu(1)–Cl(2)	2.2485(7)			
Cu(1)–O(21)		2.250(2)		
$[Cu(L1)Cl]_2·H_2O$ (**2**)				
Cu(1)–N(10)	2.024(3)		169.07(9);	82.02(13)–
Cu(1)–N(11)	2.001(3)		171.89(13)	99.11(9)
Cu(1)–O(21)	1.891(3)			
Cu(1)–Cl(1)	2.3028(10)			
Cu(1)–Cl(1)[1]		2.7062(11)		
Cu(2)–N(30)	2.003(3)		169.14(13);	82.72(13)–
Cu(2)–N(31)	1.997(3)		173.05(10)	95.21(3)
Cu(2)–O(41)	1.906(3)			
Cu(2)–Cl(2)	2.2898(10)			
Cu(2)–Cl(2)[2]		2.6561(10)		
$[Cu(HL2)Cl_2]_2·2DMF$ (**3**)				
Cu(1)–N(1)	2.0329(16)		155.05(5);	80.61(6)–
Cu(1)–N(20)	2.0420(16)		173.05(5)	109.390(18)
Cu(1)–Cl(1)	2.2767(5)			
Cu(1)–Cl(2)	2.2501(5)			
Cu(1)–Cl(1)[3]		2.6258(5)		
$[Cu(HL2)_2Cl]_nCl_n·2nH_2O$ (**4**)				
Cu(1)–N(11)	2.0267(15)		175.53(6);	75.26(6)–
Cu(1)–N(21)	2.0133(15)		173.67(4)	107.72(6)
Cu(1)–N(120)	2.0643(15)			
Cu(1)–Cl(1)	2.2569(5)			
Cu(1)–N(220)		2.4079(15)		
$[Cu(L3)Cl]_n$ (**5**)				
Cu(1)–N(1)	2.016(6)		157.24(18);	79.7(2)–
Cu(1)–N(20)	2.069(5)		164.97(19)	101.95(13)
Cu(1)–O(21)[4]	1.979(4)			
Cu(1)–O(22)[5]	1.980(4)			
Cu(1)–Cl(1)		2.4099(18)		

[a] Symmetry transformations used to generate equivalent atoms: [1] -x,-y,1-z; [2] 1-x,1-y,2-z; [3] 1-x,2-y,1-z; [4] x-1/2,1/2-y,z-1/2; [5] 3/2-x,1/2-y,1-z.

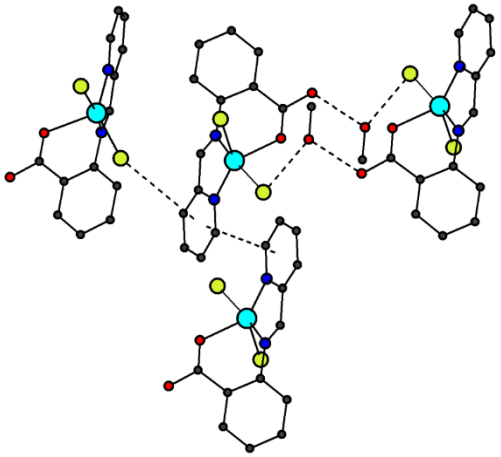

Figure 2. Fragment of crystal packing of **1** showing the hydrogen bonding, π···Cl and π···π noncovalent interactions between $Cu(HL1)Cl_2$ molecules. The intermolecular H bonds as well as noncovalent interactions are shown as dashed lines; H atoms are omitted.

Table 2. Geometry of hydrogen bonds for **1–4** (Å and °)[a]

D–H···A	d(D–H)	d(H···A)	d(D···A)	∠(DHA)
$Cu(HL1)Cl_2·CH_3OH$ (**1**)				
O(22)–H(22)···O(1)	0.835(19)	1.76(2)	2.587(3)	171(4)
O(1)–H(1)···Cl(2)[1]	0.828(19)	2.31(2)	3.129(2)	170(4)
$[Cu(L1)Cl]_2·H_2O$ (**2**)				
O(1)–H(1A)···O(42)	0.81(2)	2.06(2)	2.864(4)	169(7)
O(1)–H(1B)···O(42)[2]	0.821(19)	2.07(2)	2.891(5)	176(5)
$[Cu(HL2)Cl_2]_2·2DMF$ (**3**)				
O(21)–H(21O)···O(10)	0.811(17)	1.773(16)	2.555(2)	162(3)
$[Cu(HL2)_2Cl]_nCl_n·2nH_2O$ (**4**)				
O(121)–H(121)···O(2)	0.82	1.79	2.592(2)	163.9
O(221)–H(221)···Cl(2)	0.82	2.19	2.9899(15)	163.7
O(1)–H(1AO)···Cl(2)[3]	0.808(18)	2.38(2)	3.172(2)	168(4)
O(1)–H(1BO)···Cl(2)	0.832(17)	2.38(2)	3.193(2)	167(4)

[a] Symmetry transformations used to generate equivalent atoms: [1] –x, –y, 1–z; [2] 1–x, –y, 2–z , [3] 1–x, 2–y, –z.

*[Cu(L1)Cl]$_2$·H$_2$O (**2**)*

The compound crystallizes in the triclinic space group $P\bar{1}$; the unit cell contains two independent dimeric molecules, both of which lie on crystallographic inversion centers. There are no significant differences between the two molecules (Fig. 1, Table 1). The copper atoms are square pyramidal (τ = 0.05 and 0.07), with N10, N11, Cl1 and O21 (Cu1) and N30, N31, Cl2 and O41 (Cu2) in the basal planes with the apical atoms being the centrosymmetrically related Cl atoms.

The Cu–Cl bonds to those Cl atoms [2.7062(11), 2.6561(10) Å] are longer than bonds to the Cl atoms in the basal planes [2.3028(10), 2.2898(10) Å]. The bond distances and angles are within the usual range for this type of compound (see Discussion). The fused five- and six-membered rings of $L1^-$ groups for both dimers in **2** are virtually coplanar [dihedral angles for Cu1 and Cu2 are 3.31 and 1.47°, respectively]. Cu···Cu separations in the dimers are about 3.51 Å (Cu1) and 3.35 Å (Cu2).

The main difference between Cu1 and Cu2 arises from the involvement of the Cu2 based dimers in hydrogen bonds to water molecules. The water molecule forms H-bonds with the uncoordinated carboxylate oxygen atom O(42) and also to the same atom on a centrosymmetrically related dimeric molecule to form a one-dimensional hydrogen bonded polymer propagating along the *b* axis (Fig. 3, Table 2). In the crystal lattice, the layers built of hydrogen-bonding polymers in the *ab* plane alternate with parallel layers of loose Cu1 based dimers along the *c* axis. The offset face-centered aromatic stacking between the layers is very weak (the ring centroid distances are around 3.62 and 3.73 Å).

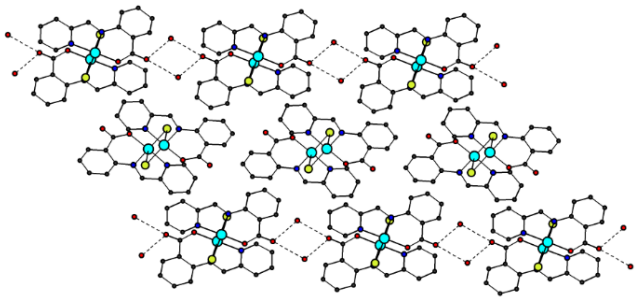

Figure 3. Crystal packing of **2** showing layered arrangement of Cu1 and Cu2 based dimers in the *bc* plane with intermolecular hydrogen bonds between the Cu2 based dimers and water molecules shown as dashed lines. H atoms are omitted for clarity.

*[Cu(HL2)Cl$_2$]$_2$·2DMF (**3**)*

The compound crystallizes in the triclinic space group $P\bar{1}$; the dimeric molecule is situated on a crystallographic inversion. The coordination about the Cu atom can be described as distorted square pyramidal (τ = 0.30), the base consisting of the two chlorine atoms, Cl1, Cl2 and the two nitrogen atoms, N1, N20 from the bidentate chelate HL2 (Fig. 1, Table 1). Bond parameters are unexceptional. The apical position is occupied by the centrosymmetrically related chlorine Cl1' of the dimer. This apical Cu1–Cl1' bond is elongated at 2.6258(5) Å compared to the Cu1–Cl1 bond length of 2.2767(5) Å. The *trans* angles of the base are N1–Cu1–Cl2 155.05(5)° and N20–Cu1–Cl1 173.05(5)°. The Cu···Cu separation in the dimer is about 3.38 Å. In contrast to HL1 in **1**, the carboxylic group of HL2 in **3** and **4** (see below) stays uncoordinated. Among the relatively few reported metal complexes of HL2, the ligand demonstrates the same coordination mode both in monomeric Pd(II),[14a] Ru(II)[14b] coordination compounds and Mn(I)[14c] and W(0)[14d] carbonyl derivatives. In the case of the trimethyl Sn compound, $Sn(CH_3)_3(H_2O)(L2)$, the carboxylate group becomes monodentate to the tin center.[14e]

In the crystal lattice of **3**, the dimers are arranged in stacks propagating along the *a* axis with the minimum Cu···Cu distance inside the stack being 5.38 Å (Fig. S6). The neighboring benzene and pyridyl rings along the stack are twisted by 33.08° with respect to each other with the ring centroid distance of 4.07 Å, too great for effective π–overlap. The solvent DMF molecules are situated between the stacks of dimers; there is a hydrogen bond between the carboxylic acid group of HL2 and the oxygen atom of the DMF molecule (Table 2).

*[Cu(HL2)$_2$Cl]$_n$Cl$_n$·2nH$_2$O (**4**)*

The compound crystallizes in the monoclinic space group $P2_1/n$; the asymmetric unit consists of one cation $[Cu(HL2)_2Cl]^+$, chloride anion and a water molecule of crystallization. In contrast to **3**, the copper atom in **4** accommodates two neutral Schiff base ligands in its coordination sphere; the former are not symmetry related. The metal atom is square pyramidal (τ = 0.03), with the Cu–N distances in the basal plane lying in the range 2.0133(15)–2.0643(15) Å and the distance to the apical atom, Cu1-N220 = 2.4079(15) Å, being significantly elongated (Fig. 1, Table 1). There is also a weak interaction to the coordinated Cl atom of the molecule related by the crystallographic 2_1-screw axis, Cu1–Cl1 [1/2-x, y-1/2, 1/2-z] at 2.9810(5) Å forming a one-dimensional helical structure along the *b* axis (Fig. 4). The second Cl atom, Cl2, is not bonded to the metal center. Although the hydrogen atoms of water molecule 2 were not located, other hydrogen bonding interactions are clearly present. The carboxylic groups are hydrogen bonded to the uncoordinated Cl atom, Cl2, and O2. Water molecule 1 forms hydrogen bonds to Cl2 and to a centrosymmetrically-related Cl2. Hydrogen bonding details are listed in Table 2. The closest Cu···Cu separation in the crystal lattice is about 4.7 Å. Considering the ring centroid distance of 3.97 Å between the adjacent aromatic rings in the chain appreciable π···π stacking can be ruled out.

Complex **4** is distinguished by a very large difference between the two Cu–Cl bond lengths [2.2569(5) and 2.9810(5) Å] compared with other monochloro-bridged copper(II) chains.[15] A polynuclear chain built with alternating short and long Cu–Cl distances of 2.365 and 2.751 Å, respectively, is found in Cu(ImH)Cl$_2$ (ImH = imidazole).[15a] In [Cu(2pymehist)Cl](ClO$_4$), where 2pymehist is 2-(4-imidazolyl)-ethylimino-6-methylpyridine, this difference is even smaller [2.322(2) and 2.614(2) Å].[15b] Nevertheless, a magnetic exchange interaction observed for **4** (see Magnetic Studies) should be transmitted through a very weakly coordinated μ-Cl$^-$ ligand.

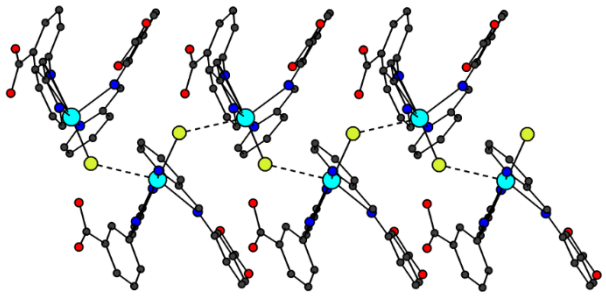

Figure 4. One-dimensional chain formed by weak Cu–Cl coordination bonding in complex **4** along the *b* axis.

*[Cu(L3)Cl]$_n$ (**5**)*

The compound crystallizes in the monoclinic space group *C*2/*c*; it is a one-dimensional polymer in the (-1 0 1) direction. The Cu

atom is bound to the chlorine atom and the pyridyl and imine nitrogen atoms of the ligand. It is also bonded to two carboxylate oxygen atoms from the two adjacent ligands, O21 through the *c*-glide and O22 through an inversion center, thus forming the polymer. The polymer consists of double strands of 4-N-(2'-pyridylimine)benzoic acid ligands bonded to the copper atoms. The polymer is not linear but is bent at the copper atoms to form a zigzag arrangement (Fig. 5). The dihedral angle between the planes generated by each set of four copper atoms is 63.43(2)°. The coordination around the copper atom is square pyramidal with the chlorine at the apex; the Cu atom is displaced 0.30 Å from the basal plane in the direction of the Cl atom (Table 1). The two copper atoms are bridged by two bidentate-bridging carboxylate groups in a syn–syn conformation to form a dimeric unit with a Cu···Cu separation of about 3.33 Å. Partial paddlewheel motifs $Cu_2(RCOO)_x$ with x ranging from 1 to 3 have been reported.[16] Structural examples for both x = 1 and x = 2 are found in the family of copper(II) complexes derived from the combination of the succinamate(–1) ligand with aromatic N,N'-chelates.[16c] The Cu···Cu distances in the latter, that vary from 2.98 to 3.22 Å, are somewhat shorter compared with **5**. In the case of $Cu_2(tzn)(OAc)_3$ [Htzn = 1,3-bis(2-carboxymethyl)benzene triazene, x = 3][16b] the Cu···Cu separation is even less than that for the "parent" dicopper tetraacetate, 2.53 vs. 2.61 Å,[17] respectively.

The double stranded polymer of **5** is reinforced by π···π stacking between the parallel benzene rings with the ring centroid distance of 3.42 Å.

Remarkably, the known solvatomorph of **5**, $[Cu_2(L3)_2Cl_2]_n \cdot 3nH_2O$ (**6**),[18] demonstrates a completely different connectivity with the deprotonated Schiff base ligand acting as a bridge with its two nitrogen atoms chelating to a Cu center of a Cu_2Cl_2 ring and its carboxylate oxygen atom coordinating in a monodentate mode to a copper atom of another Cu_2Cl_2 ring. As a result, the four-membered Cu_2Cl_2 rings in **6** are linked into a two-dimensional layer.

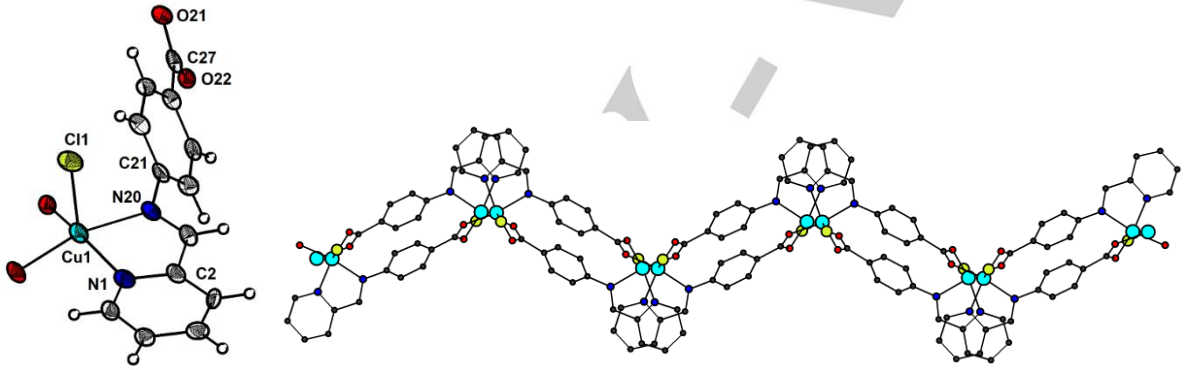

Figure 5. Fragment of the crystal structure of **5** with principal labelling and displacement ellipsoids for non-H atoms drawn at the 50% probability level (left). One-dimensional double stranded polymer formed by Cu–O coordination bonding in complex **5** projected oblique to the *b* axis (right).

EPR spectra

The X-band polycrystalline EPR spectra of **1**–**3** (Fig. 6, Table 3) show typical axial patterns with no resolved hyperfine structure. The spectra are almost temperature independent with a subtle change of their shapes seen between 295 and 77 K. The axial symmetry characteristics of **1**–**3** with a $g_{\parallel} > g_{\perp}$ relation (Table 3) confirm a square-pyramidal coordination geometry for these complexes suggested by the structural data. The X-band polycrystalline EPR spectra of **4** at RT and 77 K suggest a rhombic pattern of the *g* tensor ($g_3 > g_2 > g_1$) (Fig. 6, Table 3) and thus the ground state of Cu(II) with significant contribution from the d_{z^2} molecular orbital. This does not stay in line with the square-pyramidal copper polyhedron, for which the τ value is close to 0. Therefore, the experimental *g* values were tested to decide if they are actually molecular by the parameter *G*:[19]

$$G = (g_z - g_0)/[1/2(g_x + g_y) - g_0]$$

which lies in the 4.4–4.9 range when the *g* values are equal to molecular values. In the case of **4**, the calculated *G* value is 2.74 strongly implying that the observed EPR features arise from the coupling of *g*-tensors from differently oriented Cu(II) coordination polyhedra in the solid state rather than from a d_{z^2} contribution to the copper(II) ground state.[20a] Hence, the ground state of Cu(II) in **4** is expected to be dominated by the $d_{x^2-y^2}$ molecular orbital and this is further supported by DFT calculations.

Such EPR behaviour is not unique for square-pyramidal copper(II) complexes with misaligned local molecular axes. The X-band EPR spectrum of the polycrystalline compound $[Cu_2Cl_4(L)]\cdot 2CH_3CN$ with substituted 1,3,5-triazine-2,4,6-triamine ligand L with $g_1 = 2.05$, $g_2 = 2.11$ and $g_3 = 2.24$ was interpreted by the authors in terms of a rhombic symmetry.[20b] However, *G* value calculated by us from these experimental data is equal to 3.06 indicating that the effective *g* values are not molecular. Our inspection of the crystal structure reveals that while the two Cu(II) centers with the same CuN_3Cl_2 donor set in the molecule of $[Cu_2Cl_4(L)]\cdot 2CH_3CN$ are symmetry related, their local molecular axes are profoundly misaligned. In the crystal structure of $[Cu(mpppa)Cl_2]$ [mpppa – N-methyl-N-((6-pivaloylamido-2-pyridyl)methyl)-N-(2-pyridylethyl)amine], the complex molecules with a CuN_3Cl_2 chromophore are arranged in a 1D helical chain via intermolecular C–H···Cl hydrogen-bonding interactions in the way similar to **4**.[20c] Three distinct *g* values: $g_1 = 2.185$, $g_2 = 2.140$, and $g_3 = 2.068$ observed in its powder EPR

spectrum were also interpreted as arising from a rhombic pattern. The calculated *G* value of 1.80 does not support this assignment.

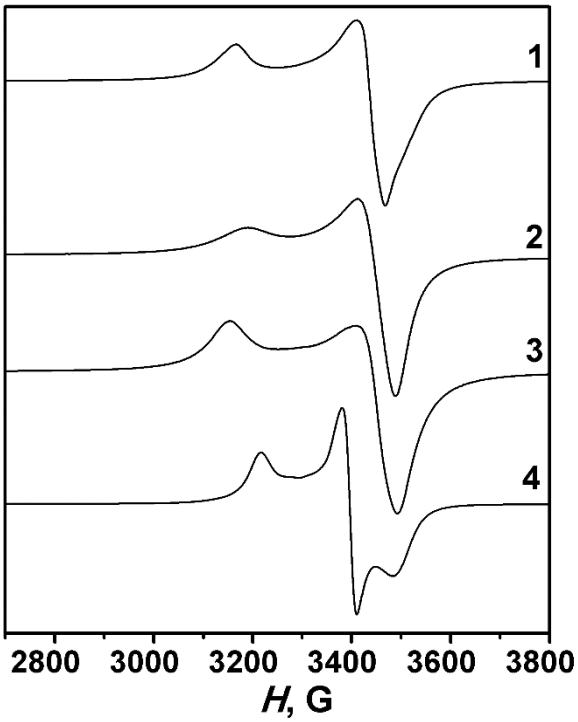

Figure 6. X-band powder EPR spectra of $Cu(HL1)Cl_2 \cdot CH_3OH$ (**1**), $[Cu(L1)Cl]_2 \cdot H_2O$ (**2**), $[Cu(HL2)Cl_2]_2 \cdot 2DMF$ (**3**) and $[Cu(HL2)_2Cl]_nCl_n \cdot 2nH_2O$ (**4**) at 77 K.

The polycrystalline Cu(II) complex of the asymmetric Schiff base ligand derived from 2-(2-aminoethyl)pyridine and 3,5-di-*tert*-butyl-4-hydroxybenzaldehyde with a CuN_2O_3 donor set showed three signals in the Q-band EPR spectrum with observed *g* values of 2.180, 2.115 and 2.059.[20d] The spectrum was considered a result of cooperative effects due to magnetic exchange between the non-equivalent paramagnetic centers with the observed values of *g* components caused by coupling of the *g* matrixes. The calculated *G* value of 2.10 is in accord with the conclusion made by the authors.

The EPR data show no indication of exchange interactions between copper ions in **1**–**4** in the range 295–77 K in agreement with the experimental magnetic data and calculated exchange coupling constants (see below).

Table 3. Parameters of powder EPR spectra of **1**–**4** at 77 K

Complex	g_1	g_2	g_3
1	2.078	2.078	2.243
2	2.061	2.061	2.235
3	2.069	2.069	2.252
4*	2.053	2.103	2.210

* these are not the molecular *g* parameters, see text for details

The polycrystalline powder EPR spectrum of **5** at room temperature is dominated by a broad isotropic signal centered at about g_{eff} = 2.16 ($\Delta Hpp \approx$ 1500 G) (Fig. 7). At 77 K **5** shows a characteristic spin-triplet EPR spectrum with four well-resolved features at 1400, 2600, 3200 and 3800 cm^{-1}. The feature at 3200 G most certainly originates from a monomeric Cu(II) impurity, which is always present in dinuclear species and the absorption at low field (1400 G) is the $\Delta M_S = \pm 2$ transition. The fine structure components of the spin-triplet state coming from the first excited state of the antiferromagnetic di-copper entity were simulated using the spin-Hamiltonian parameters for $S = 1$, $g_x = 2.08$, $g_y = 2.11$, $g_z = 2.37$ and the value of the zero-field splitting parameter *D* of 0.137 cm^{-1} (1470 G). The contribution of paramagnetic impurities was estimated by the magnetic data fitting.

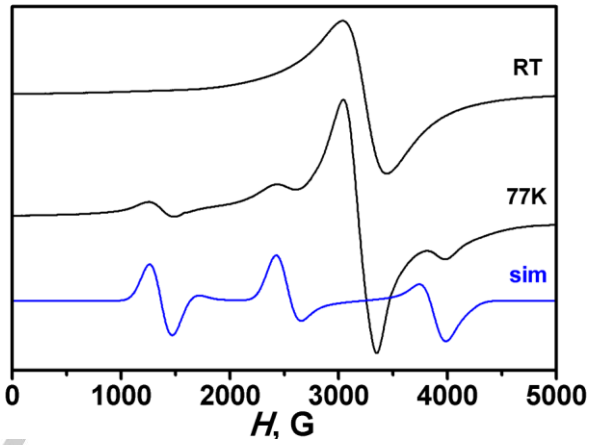

Figure 7. X-band EPR spectra of the polycrystalline sample $[Cu(L3)Cl]_n$ (**5**) at room temperature and 77 K, sim – simulated spectrum for S = 1 with parameters given in the text.

Magnetic studies

The results of susceptibility measurements of complexes **1**–**5** are illustrated in Fig. 8 in the form χ_m, $\chi_m T$ versus *T* (χ_m being the corrected molar magnetic susceptibility per one metal ion and *T* is absolute temperature). Temperature dependences of reciprocal susceptibility χ_m^{-1} are also presented in the insets.

Experimental data fitting results for **1**–**4**

Magnetic properties of **1**–**4** at higher temperatures are very similar, the $\chi_m T$ values at the room temperature are almost equal: 0.428 (μ_{eff} = 1.85 B.M.), 0.422 (μ_{eff} = 1.84 B.M.), 0.440 (μ_{eff} = 1.88 B.M.) and 0.427 cm^3 K mol^{-1} (μ_{eff} = 1.85 B.M.) for **1**–**4**, respectively. These values practically do not change with lowering temperature down to 25 K, and then decrease (**1**–**3**) or increase (**4**) sharply reaching 0.220 (μ_{eff} = 1.33 B.M.), 0.286 (μ_{eff} = 1.51 B.M.), 0.165 (μ_{eff} = 1.15 B.M.) and 1.15 cm^3 K mol^{-1} (μ_{eff} = 3.04 B.M.) for **1**–**4**, respectively, at 1.8 K. This behavior indicates the occurrence of weak antiferromagnetic (**1**–**3**) and

ferromagnetic (**4**) interactions between copper ions at very low temperatures.

Taking into account the dimeric structure of **2** and **3** their magnetic data have been analyzed using Bleaney-Bowers equation based on the Hamiltonian $H = \sum J_{ij} S_i S_j$:

$$\chi_m = \frac{N\beta^2 g^2}{3kT}\left[1 + \frac{1}{3}exp\left(\frac{-J}{kT}\right)\right]^{-1} \quad (1)$$

where the J value (singlet-triplet energy gap) characterizes intradimer interactions, N is the Avogadro number, g is the spectroscopic splitting factor, β is the Bohr magneton, and k is the Boltzmann constant. While the molecular structure of complex **1** is monomeric, there are several possible pathways for magnetic exchange in the crystal through noncovalent interactions (Fig. 2). The susceptibility *versus* temperature plot of **1** was thus fitted with a dimer model. The best-fit parameters obtained are: g = 2.12, J = –2.3 cm^{-1}, R = 1.2 × 10^{-3}; g = 2.15, J = –1.4 cm–1, R = 3.6 × 10^{-5} and g = 2.16, J = –4.0 cm^{-1}, R = 7.9 × 10^{-5} for **1**, **2** and **3**, respectively. Magnetic susceptibilities for these compounds obey Curie-Weiss low with the parameters: C = 0.431 cm^3 K mol^{-1}, θ = –1.9 K; C = 0.424 cm^3 K mol^{-1}, θ = –0.9 K and C = 0.464 cm^3 K mol^{-1}, θ = –3.07 K for **1**, **2** and **3**, respectively. Magnetization data for **3** at 2 K were collected in the range 0–50 000 G. The experimental data lie below the $M/N\beta$ calculated value for an isolated S = 1/2 ion, thus confirming the antiferromagnetic coupling in the complex (Fig. S7).

The magnetic data of compound **4** have been fitted to the numerical expression of Baker *et al.*[21] for a ferromagnetic S = 1/2 regular chain:

$$\chi_{\mathrm{m}} = \frac{Ng^2\beta^2}{4kT}\left[\frac{A}{B}\right]^{2/3} \quad (2)$$

where A = 1.0 + 5.7979916y + 16.902653y^2 + 29.376885y^3 + 29.832959y^4 + 14.036918y^5, B = 1.0 + 2.7979916y + 7.0086780y^2 + 8.6538644y^3 + 4.5743114y^4 with $y = J/2kT$ and with the spin Hamiltonian defined as $H = -J\sum_{i=1}^{n-1} S_i S_{i+1}$. J is the intrachain magnetic coupling parameter and other symbols have their usual meaning. A least-squares fit of the susceptibility data for complex **4** gives g = 2.16, J = 3.27 cm^{-1}, R = 2.0 × 10^{-3}.

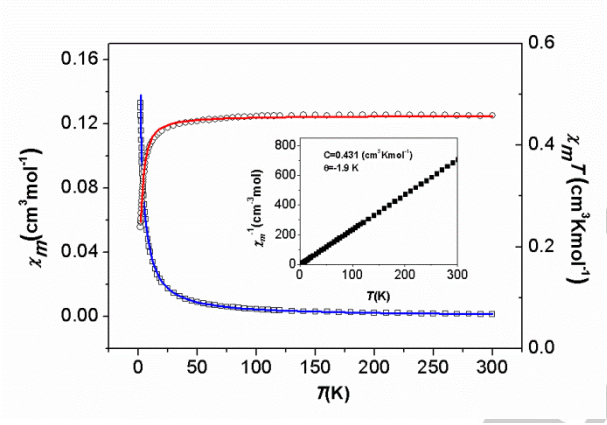

(**1**)

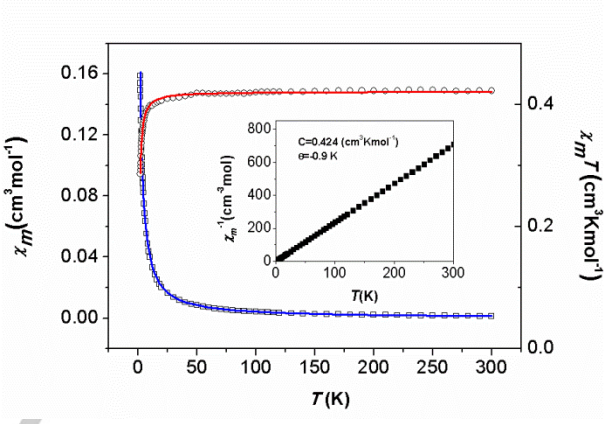

(**2**)

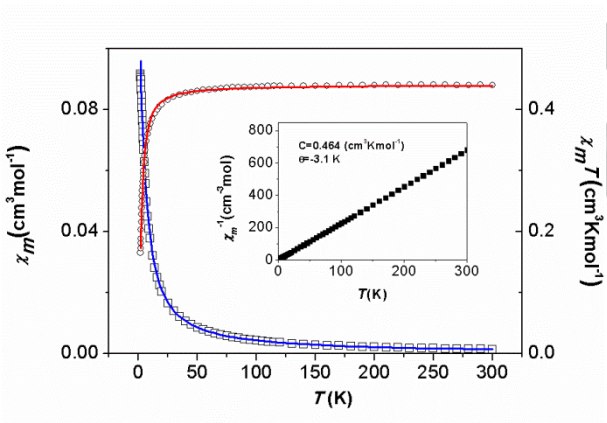

(**3**)

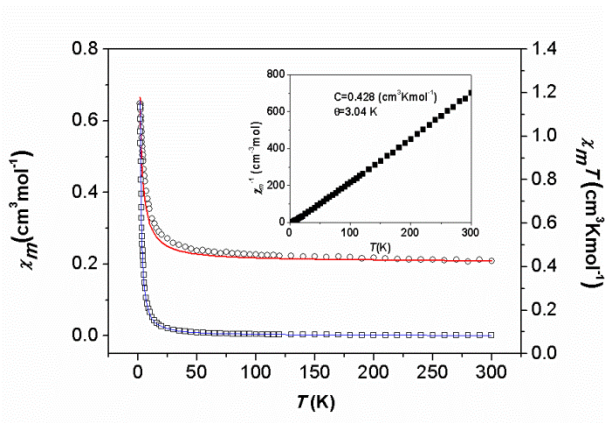

(**4**)

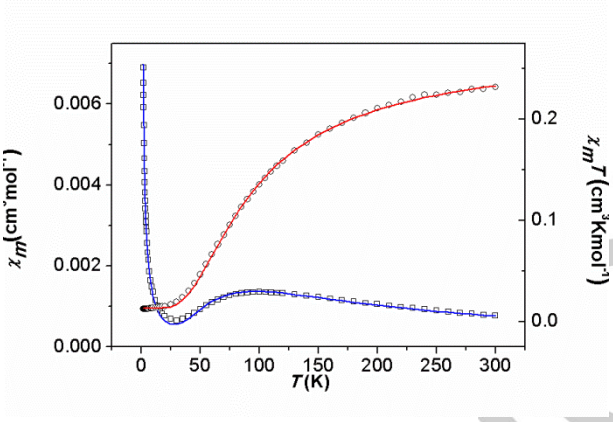

(5)

Figure 8. Temperature dependences of χ_m (□) and $\chi_m T$ (○) for Cu(HL1)Cl_2·CH_3OH (**1**), $[Cu(L1)Cl]_2$·H_2O (**2**), $[Cu(HL2)Cl_2]_2$·2DMF (**3**), $[Cu(HL2)_2Cl]_nCl_n$·2nH_2O (**4**) and $[Cu(L3)Cl]_n$ (**5**). Solid lines represent the best fit, insets show χ_m^{-1} vs. *T* relation.

Experimental data fitting results for ***5***

The susceptibility data for **5** show a broad maximum at about 100 K, then decrease gradually till 25 K and further increase abruptly at lower temperatures (Fig. 7). Such a dependence is characteristic of two antiferromagnetically coupled copper(II) ions. The increase of susceptibility below 25 K suggests the presence of a monomeric impurity in **5**. The $\chi_m T$ values of 0.232 (μ_{eff} = 1.36 B.M.) at room temperature is lower than the theoretical value corresponding to *S* = 1/2 (1.73 B.M.) and drops down to 0.0124 cm^3 mol^{-1} K (μ_{eff} = 0.32 B.M.) at 1.8 K confirming antiferromagnetic exchange between the copper ions. The modified Bleaney-Bowers equation (3) that takes into account the presence of a monomeric impurity was used to fit the susceptibility data:

$$\chi_m = \frac{Ng^2\beta^2}{kT\left[3+\exp\left(-\frac{J}{kT}\right)\right]}(1-x) + \frac{Ng^2\beta^2}{4kT}x \quad (3)$$

in which *x* is the molar fraction of noncoupled species.[22]

The fitting procedure using equation (3) results in *J* = –118 cm^{-1}, *g* = 2.18, monomeric impurity *x* = 3%, *R* = 5.9 × 10^{-5}. The temperature T_{max} = 112 K, which was calculated from the obtained singlet-triplet energy gap *J* = –118 cm^{-1} using the relation $|J|/kT_{max}$ = 1.599, is in good accordance with T_{max} observed in the experimental data.

Theoretical calculations

The 3d orbitals of a copper(II) ion located in an octahedral ligand field undergo splitting into the t_{2g} and e_g set. Allocation of nine electrons among them places three electrons in the e_g series. Such an electronic configuration is unstable due to the Jahn-Teller effect, which lifts the degeneracy and lowers the molecular symmetry. If the resulting molecular structure becomes elongated octahedral, square pyramidal or square planar, then the unpaired electron occupies the $d_{x^2-y^2}$ orbital.[19,23] As revealed by the DFT computations (Fig. 9), the singly occupied molecular orbitals (SOMOs) for complexes **1**–**5** are not pure $d_{x^2-y^2}$ but $d_{x^2-y^2}$ involved in the σ-antibonding interaction with the orbitals of ligands. According to the Löwdin reduced orbital populations at the B3LYP/def2-TZVP theory level the SOMO of **1** is only 51% of $d_{x^2-y^2}$ in character. This result is consistent with data obtained for square-planar $[CuCl_4]^{2-}$ (61%),[19] although it is lower due to the distorted structure of **1** allowing for small contributions from the other d-type orbitals. The substantial contributions from the orbitals of ligands to the SOMOs of **1**–**5** bring about the significant spin density flow from the central copper(II) ions towards the donor atoms of ligands. This is illustrated with the Löwdin spin populations in Fig. 9.

In a dinuclear Cu(II) complex with the magnetic orbitals (SOMOs) being of the $d_{x^2-y^2}$ type, the symmetric and antisymmetric combinations of these orbitals are possible and the singlet–triplet energy gap, hence the *J* parameter, becomes dependent on the relative stability of the two combinations.[24] The magnetic orbitals predicted at the B3LYP level for dinuclear **2**, **3** and **5** are in accord with these expectation. For each of these three complexes the SOMO#1 is the antisymmetric and the SOMO#2 the symmetric combination (Fig. 9). Only for **4** the two combinations were not predicted. Instead, each of the magnetic orbitals is located on one Cu atom. These can be explained by the noticeably larger Cu···Cu distance in **4** (4.669 Å) in comparison with **2** (3.506 Å), **3** (3.377 Å) and **5** (3.327 Å).

The intradimer exchange couplings parameters *J* were calculated for complexes **2**–**5** and are listed in Table 4. Usually, Broken Symmetry (BS) DFT calculations can be reasonably accurate when compared to the experimentally determined *J* values.[24c,25] Before further discussion, it is advisable to briefly compare the performance of the three used functionals, namely the B3LYP, TPSSh and B97D, and various basis sets. The results obtained here with the TPSSh method clearly indicate a stronger magnetic superexchange interaction in comparison with the functional B3LYP. This is particularly evident if the *J* values computed for **5** are compared. The functional B97D predicted the significantly greater *J* values for **3**, **4** and **5**. Interestingly, the predicted *J* values were found to change only slightly with the basis set size, but this alteration brings the computed values closer to the ones determined experimentally. However, even the results obtained with use of valence double-zeta basis sets (def2-SVP and cc-pVDZ) are reasonably accurate.

In general, all the intradimer exchange coupling constants calculated at the hybrid DFT theory level (B3LYP and TPSSh) stay fairly close to their experimental counterparts. In contrast, the functional B97D, which was shown successful in the exploration of the weak π···π and CH···π interactions in Cu dimers[8a], seems to lack accuracy here due to the absence of the Hartree–Fock (HF) exchange. It appeared unsuitable for the calculation of intradimer exchange couplings parameters in the present study.

For complexes **2**–**4** only a very weak exchange interaction between the Cu(II) ions was predicted with B3LYP and TPSSh. Although for **2** and **3** neither of these two functionals were able to provide the right sign of the *J* parameter, the absolute error of several cm^{-1} in the *J* value can be considered most satisfactory when the coupling is weak. In the case of **5**, the *J* values are noticeably overestimated, but this should be expected at the BS DFT theory level.[25a,b,g] Significantly better results were obtained for **5** with the DDCI2 and DDCI3 *ab initio* methods and the combined B3LYP/DDCI3 approach.

In order to identify the paths of exchange coupling via noncovalent intermolecular interactions in **1**, three computational models were taken under investigation, that is the mediation through hydrogen bonds engaging the methanol molecules (labeled as H···O), the π···π interaction between the HL1 ligands, and π···Cl interaction (Fig. 10). It is noteworthy that in this regard the functional B97D performed satisfactorily in the prediction of *J*. This supports the previous findings of Singh and Rajaraman.[8a] In Fig. 10 the spin densities for noncovalently interacting dimers are shown. Noticeably, along every one of the three interaction pathsways, there is the spin density concentration and this suggests that the magnetic coupling can be transmitted along them.

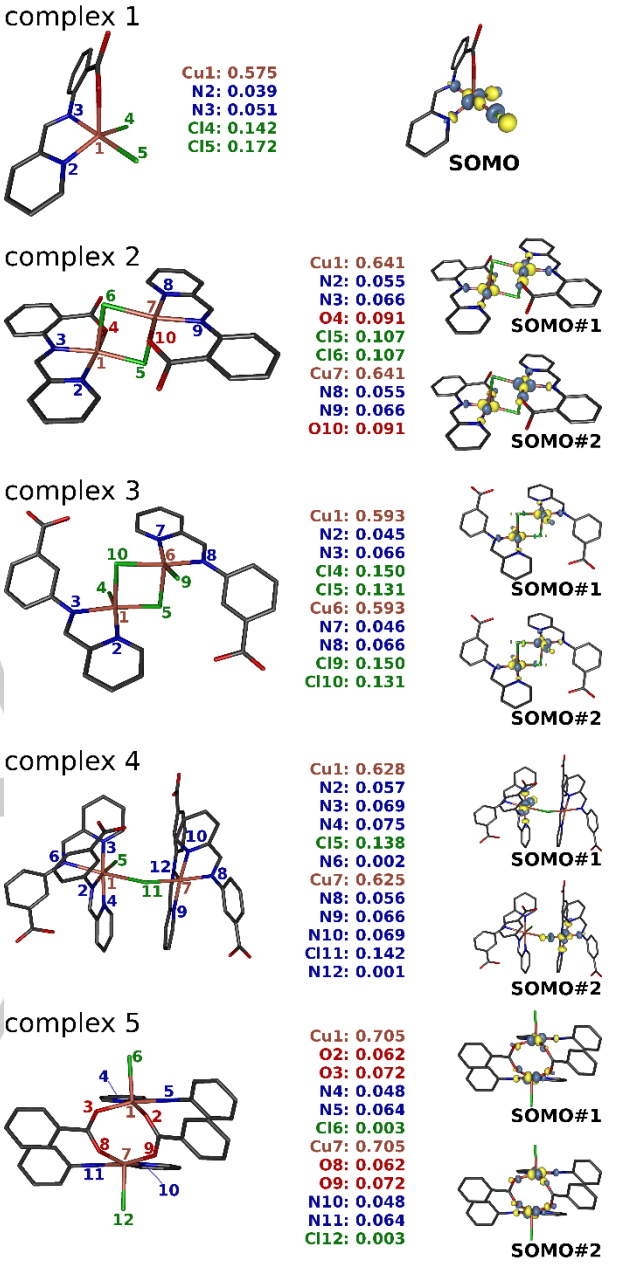

Figure 9. Molecular structures of model systems used in the computational study, Löwdin spin populations and isosurfaces of SOMOs. Hydrogen atoms were removed for clarity.

Table 4. Exchange coupling parameters *J* (cm^{-1}) computed with three density functionals, *ab initio* methods and combined approach, the last calculated as *J* = *J(B3LYP/def2-QZVPP) + [J(DDCI3/cc-pVDZ) – J(B3LYP/cc-pVDZ)]*

	method	basis set	*J*	method	basis set	*J*	method	basis set	*J*
Complex 1	B3LYP	def2-SVP	0.00	TPSSh	def2-SVP	0.04	B97D	def2-SVP	-0.04
(H···O)		def2-TZVP	-0.32		def2-TZVP	0.02		def2-TZVP	-0.02

		def2-TZVPP	-0.50		def2-TZVPP	-0.10		def2-TZVPP	-0.04
		def2-QZVPP	-0.26		def2-QZVPP	-0.10		def2-QZVPP	-0.22
Complex 1	B3LYP	def2-SVP	-0.42	TPSSh	def2-SVP	-0.34	B97D	def2-SVP	-1.18
(π···π)		def2-TZVP	-0.38		def2-TZVP	-0.42		def2-TZVP	--1.22
		def2-TZVPP	-0.26		def2-TZVPP	-0.48		def2-TZVPP	-1.20
		def2-QZVPP	-0.14		def2-QZVPP	-0.32		def2-QZVPP	-1.56
Complex 1	B3LYP	def2-SVP	0.74	TPSSh	def2-SVP	1.62	B97D	def2-SVP	2.10
(π···Cl)		def2-TZVP	0.52		def2-TZVP	1.08		def2-TZVP	1.98
		def2-TZVPP	0.50		def2-TZVPP	1.04		def2-TZVPP	1.95
		def2-QZVPP	0.52		def2-QZVPP	1.08		def2-QZVPP	1.92
Complex 2	B3LYP	def2-SVP	11.0	TPSSh	def2-SVP	7.3	B97D	def2-SVP	1.16
		def2-TZVP	10.6		def2-TZVP	7.0		def2-TZVP	1.02
		def2-TZVPP	10.6		def2-TZVPP	14.0		def2-TZVPP	0.80
		def2-QZVPP	9.6		def2-QZVPP	13.4		def2-QZVPP	0.78
Complex 3	B3LYP	def2-SVP	7.0	TPSSh	def2-SVP	7.5	B97D	def2-SVP	31.48
		def2-TZVP	3.6		def2-TZVP	4.0		def2-TZVP	34.88
		def2-TZVPP	3.6		def2-TZVPP	3.8		def2-TZVPP	34.22
		def2-QZVPP	3.3		def2-QZVPP	3.8		def2-QZVPP	33.52
Complex 4	B3LYP	def2-SVP	18.0	TPSSh	def2-SVP	28.2	B97D	def2-SVP	57.98
		def2-TZVP	17.0		def2-TZVP	26.5		def2-TZVP	63.96
		def2-TZVPP	16.4		def2-TZVPP	25.4		def2-TZVPP	61.12
		def2-QZVPP	15.9		def2-QZVPP	24.9		def2-QZVPP	60.74
Complex 5	B3LYP	def2-SVP	-211.8	TPSSh	def2-SVP	-305.8	B97D	def2-SVP	-472.61
		def2-TZVP	-210.2		def2-TZVP	-297.6		def2-TZVP	-492.60
		def2-TZVPP	-204.1		def2-TZVPP	-296.0		def2-TZVPP	-499.44
		def2-QZVPP	-201.4		def2-QZVPP	-294.2		def2-QZVPP	-497.71
		pVDZ	-209.4						
	DDCI2	pVDZ	-168.2						
	DDCI3	pVDZ	-154.0						
	B3LYP/DDCI3	def2-QZVPP/pVDZ	-146.0						

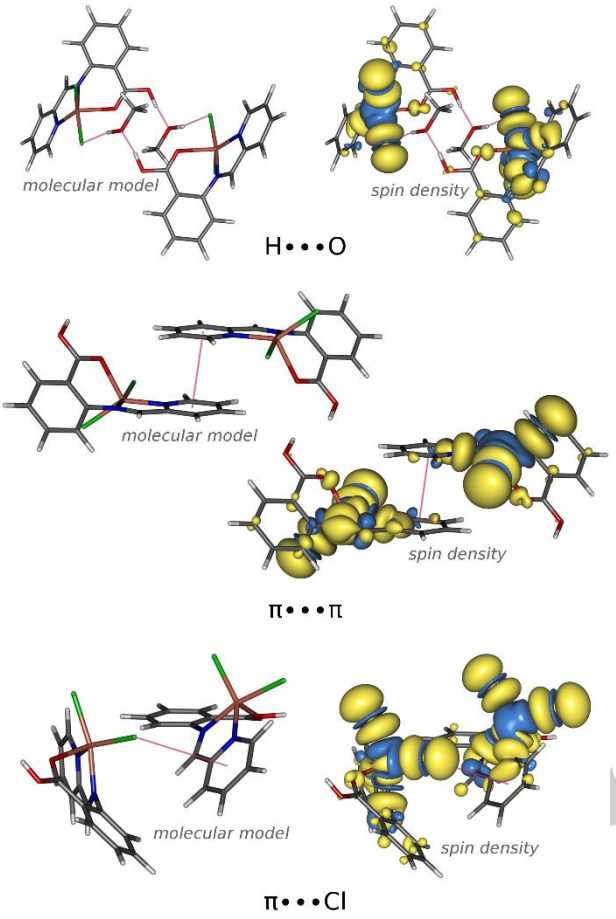

Figure 10. Molecular models used in the DFT studies of exchange coupling mediated by noncovalent intermolecular interactions in **1**; in addition spin density isosurfaces are shown (calculated at the B3LYP/def2-TZVPP theory level).

Discussion

Both the chloride ion and carboxylate group are especially prominent bridging species. Compounds **1**–**5** are peculiar examples where substituted benzoic acids and chloride ligands are combined to produce mono-, di- and polymeric complexes in which dimeric or polymeric structures are realized through bridging functions of solely chloride ligands (**2**–**4**) or carboxylate groups (**5**). While polynuclear and polymeric copper complexes of deprotonated L1 with bridging carboxylate groups are known,[13] compound **2** demonstrates that in competition with chloride anions, the latter are in favour of bridging the metal atoms. At the same time, HL1 in the neutral form seems to preclude formation of a chloro-bridged species in complex **1** by occupying the apical position at the copper atom with its carboxylic oxygen. In the case of HL2, the tridentate-chelate coordination mode cannot be realized due to sterical reasons. To the best of our knowledge copper complexes of HL2 have not been reported, however, **3** and **4** show chloro bridges to prevail over bridging through carboxylic groups as well. In the case of HL3, both options are possible, considering structures of **5** and known **6**,[18] and, what is more, simultaneous bridging of copper atoms through two chlorides and one carboxylate group of L3 can occur ($[Cu_4(L3)_2(HL3)_2Cl_4](ClO_4)_2{\cdot}2CH_3OH$,[18] **7**).

Magnetic properties of a large variety of mono-chloro- and di-chloro-bridged copper(II) complexes have been studied for over four decades with the aim to establish systematic magneto-structural correlations. There is a large body of data for Cu(μ-Cl)$_2$Cu complexes with square-pyramidal (SP) and trigonal-bipyramidal (TBP) coordination geometries. An empirical correlation between the singlet–triplet gap in such compounds and the φ/R_0 ratio, where φ is a bridging CuClCu angle and R_0 is the longer axial Cu–Cl distance in the SP geometry and the equatorial distance in the TBP geometry, was proposed by Hatfield and co-workers.[26] It was found that for 32.6 < φ/R_0 < 34.8 °/Å values, the exchange interaction is ferromagnetic and for values beyond these limits the interactions are antiferromagnetic. Many of the studied complexes having a geometry of square pyramids sharing a base-to-apex edge with parallel basal planes (SP I) are consistent with this correlation (Table 5, compounds 1–14).[27] For complex **3**, φ/R_0 value is equal to 33.0 °/Å, and the exchange is antiferromagnetic (J = –4.0 cm^{-1}). The structure of SP I complex **2**, that is also antiferromagnetic (J = –1.4 cm^{-1}), is complicated by the presence of two crystallographically independent dimers with φ/R_0 values of 31.9 and 32.8 °/Å falling into "antiferromagnetic" and "ferromagnetic" ranges. These results do not fit the trend of the Hatfield's analysis. Compounds **2** and **3** with relatively simple structures are not unique in this respect (Table 5, compounds 15–24)[18,28] emphasizing the need to take into consideration other structural factors to improve theoretical models.

For molecular complex **1** with no bridging ligands between copper atoms, the overall magnetic coupling throughout the compound is weakly antiferromagnetic in nature, with a J value of –2.3 cm^{-1}. From the crystal structure, several possible exchange pathways responsible for the type of magnetic behavior observed can be inferred: the hydrogen bonding, π···Cl and π···π noncovalent interactions. Surprisingly, the magnitude of the J value obtained in the case of noncovalent interactions in **1** is larger than that for the dichloro-bridged dimer **2** bearing the same ligand. Both hydrogen bonding[29] and π-stacking[8a,30] have been reported to propagate essentially antiferromagnetic interactions between metal centers with exchange-coupling constants provided by theoretical calculations being in good agreement with experimentally reported values. In recent years, the π···halide interaction has also been recognized as a noncovalent bonding interaction being able to mediate magnetic coupling exhibiting a ferromagnetic sign.[31] It is not obvious whether the observed coupling in **1** is due to a particular exchange pathway since various intermolecular interactions usually compete in the solid state.

Magneto-structural correlations for copper(II) mono-chloro-bridged chain compounds have not been developed in the same detail as those for the dichloro-bridged dimers due to the insufficient amount of both structurally and magnetically characterized examples.[15,28c] The relevance of various

Table 5. Structural and magnetic data for some di-μ-chloro-bridged Cu(II) complexes with SPI geometry[a]

	Complex	φ [°]	φ/R_0 [°/Å]	J [cm^{-1}]	d(Cu–Cl$_{basal}$) [Å]	R_0 [Å]	Ref.
1	$[Cu(TMSO)_2Cl_2]_2$	88.5	29.30	–16.0	2.280	3.020	[27a]
2	$[Cu(2\text{-methylpyridine})_2Cl_2]_2$	100.63	29.91	–7.4	2.287	3.364	[27b]
3	$[Cu(apyhist)Cl]_2(ClO_4)_2$	87.46	31.95	–3.09	2.271	2.737	[27c]
4	$[Cu(pmpe)Cl]_2$	89.31	32.29	–4.54	2.298	2.766	[27d]
5	$[Cu(pdon)Cl_2]_2\cdot 2DMF$	87.66	32.59	–1.16	2.2651	2.6894	[27e]
6	$[Cu(dmg)Cl_2]_2$	88.00	32.62	+0.62	2.238	2.698	[27f]
7	$[Cu(dbea)Cl_2]_2$	87.10	32.77	+5	2.298	2.735	[27g]
8	$[Cu(pz^{Ph})(opo)Cl]_2$	93.6	33.1	+8.72	2.289	2.832	[27h]
9	$[Cu(iydio)Cl]_2(ClO_4)_2$	88.81	33.4	+1.16	2.3248	2.657	[20i]
10	$[Cu(dien)Cl]_2(ClO_4)_2$	92.0/92.1	33.5_{av}	+0.4	2.313/2.266	2.770/2.735	[27j,k]
11	$[Cu(Hfsaaep)Cl]_2$	95.27	33.6	+0.30	2.308	2.846	[27l]
12	$[Cu(bpdio)Cl_2]_2$	96.68	33.99	+4.87	2.273	2.844	[27m]
13	$[Cu(pmdio)Cl]_2(ClO_4)_2$	88.2	34.17	+2.28	2.291	2.581	[27n]
14	$[Cu(2,2\text{-dimethylaziridine})_2Cl_2]_2$	93.14	34.82	–3.7	2.347	2.675	[27o]
15	$[Cu(aamo)Cl]_2$	82.9	29.52	+12.0	2.329	2.808	[28a]
16	$[Cu(pytn)Cl_2]_2$	88.6	30.49	+27.46	2.217	2.906	[28b]
17	$[Cu(L1)Cl]_2\cdot H_2O$ (**2**)	88.47/ 84.79	31.9/ 32.8	–1.4	2.303/2.290	2.706/2.656	This work
18	$[Cu(pbpe)Cl]_2(ClO_4)_2$	88.09	32.2	+6.0	2.286	2.732	[28c]
19	$[Cu_2(L3)_2Cl_2]_n\cdot 3nH_2O$ (**6**)	85.61	32.3	+4.95	2.285	2.653	[18]
20	$[Cu(Hbpmdio)Cl_2]_2(ClO_4)_2$	94.7	32.43	+10.70	2.292	2.918	[28d]
21	$[Cu_2(pmdip)_2Cl_2](ClO_4)_2$	86.44	32.74	–1.95	2.28	2.64	[28d]
22	$[\{Cu(terpy)Cl\}_2](PF_6)_2$	89.9	33.0	–5.9	2.218	2.723	[28e]
23	$[Cu(HL2)Cl_2]_2\cdot 2DMF$ (**3**)	86.76	33.0	–4.0	2.277	2.626	This work
24	$[Cu(mebta)_2Cl_2]_2$	88.1	33.5	+6.7	2.302	2.629	[28f]

[a] Ligand abbreviations: TMSO = tetramethylene sulfoxide; apyhist = (4-imidazolyl)ethylene-2-amino-1-ethylpyridine; Hpmpe = *N*-(1*H*-pyrrol-2-ylmethylene)-2-pyridineethanamine; pdon = 1,10-phenanthroline-5,6-dione; dmg = dimethylglyoxime; dbea = *N*,*N*-dimethyl,*N*'-benzyl-ethylenediamine; pz^{Ph} = 3-phenylpyrazolyl; Hopo = 2-hydroxypyridine-N-oxide; iydio = 1-(imidazol-4-ylmethyl)-1,5-diazacyclooctane; dien = diethylenetriamine; H_2fsaaep = 3-[*N*-2-(pyridylethyl)formimidoyl] salicylic acid; bpdio = 2,2-bis-(2-pyridyl)-1,3-dioxolane; pmdio = 1-(2-pyridylmethyl)-1,5-diazacyclooctane; Haamo = 8-amino-5-aza-4-methyl-3-octene-2-one; pytn = 2-(pyrazol-1-yl)-2-thiazoline; pbpe = N-{(pyrazol-1-yl)methyl}-N-benzyl-2-(pyridin-2-yl)ethanamine; bpmdio = 1,5-bis(pyridin-4-ylmethyl)-1,5-diazacyclooctane; pmdip = 1-(pyridin-2-ylmethyl)-1,4-diazacycloheptane; terpy = 2,2':6',2''-terpyridyl; mebta = methylbenzotriazole.
*J, $H = \sum J_{ij} S_i S_j$

geometrical aspects in the magnetic behavior of mono-μ-chloro–copper chains has been considered. Hatfield[32a] pointed out that overall ferromagnetic behavior can be expected for values of the φ/R_0 ratio lower than approximately 40 and higher than 57, whereas antiferromagnetic character appears when this ratio is between these two values. Landee and Greeney[32b] suggested that the L_{trans}–Cu–halide bond angle, θ, is a better parameter to assess the magnetic interaction strength. It was further shown

that θ values close to 180° favour the ferromagnetic behaviour, while an antiferromagnetic behaviour is observed for the angles smaller than 167°.[15f] It is important to note that the above correlations are valid for mono-chloro-bridged copper(II) compounds which exhibit geometries comprised between square-pyramidal and trigonal-bipyramidal. That is not the case for complex **4** in which the bridging Cl^- ion occupies an equatorial coordination site for one Cu(II) ion and the sixth, axial, position for the symmetry-generated metal center. Nevertheless, the ferromagnetic coupling in **4** seems to be accounted for by the θ value of 173.67(4)° (N120–Cu1–Cl1). It will be possible to establish the apparent magneto-structural correlation as further magnetic and structural data concerning new compounds of this kind become available.

While the majority of the compounds with copper-chloride bridges usually show small ferromagnetic or antiferromagnetic coupling constants (Table 5),[7,15,18,27,28] copper-carboxylato bridges provide a pathway for much stronger magnetic superexchange. Cu(II) is known to form molecular tetracarboxylate clusters, which contain the characteristic paddlewheel dimer. The nature of the group bonded to the carbon atom in the carboxylato bridge has a dramatic effect on the coupling constant. When the methyl group in acetate is replaced by CCl_3 *J* is reduced from –296 to less than –200 cm^{-1}, whereas its replacement with SiR_3 enhances the antiferromagnetic coupling up to –1000 cm^{-1} determined from variable-temperature ESR studies.[33] Copper paddlewheels are also ubiquitous in copper coordination polymers and MOFs.[34] The paddlewheel copper(II) carboxylate dimers based on N-(3-propanoic acid)-1,8-naphthalimide with highly organized, extended structures are diamagnetic solids at and above room temperature with *J* values that must be more negative than –600 cm^{-1}.[34a]

A partial paddlewheel structure of **5** suggests that competitive coordination of chloride ligands precludes formation of the full copper paddlewheel. Structures of closely related compounds **6** and **7** support this observation although other possibilities such as steric constraints cannot be dismissed. The magnitude of the intramolecular exchange interaction in **5** is lower compared with that for known full paddlewheels, which is consistent with the theoretical calculations that a lesser number of the carboxylato bridges and a larger distance between the two bridged Cu^{2+} ions lead to a decrease in the magnetic coupling intensity.[33]

An efficient way to interpret results of the BS DFT calculations is to perform the corresponding orbital transformation of BS determinant. This assigns the orbitals into three categories which can be chemically interpreted,[25f,35] that is (i) doubly occupied spin α and β pairs with their spatial overlap close to unity (S ≈ 1); (ii) non-orthogonal magnetic spin α and β pairs with their overlap clearly smaller than one (S < 1), and (iii) unpaired spin α orbitals. The non-orthogonal magnetic orbitals provide an image of magnetic interaction while the spatial overlap for each magnetic pair indicates the strength of the interaction that this pair mediates. The inspection of the corresponding orbitals obtained for the BS solution for **2**–**4** did not reveal the non-orthogonal magnetic pairs. This indicates that in **2**–**4** there is no efficient path for superexchange and thus the observed magnetic couplings are of minor magnitude. This is understandable since in these complexes the bridging chlorine atoms that are in the equatorial position of one Cu(II) ion occupy the axial position of the other one. Therefore, for each Cu(II) the different d orbitals participate in the interactions inside the Cu–Cl–Cu bridge, namely $d_{x^2-y^2}$ and d_{z^2}. The latter is not magnetically active and thus the exchange interactions between the two Cu(II) ions are efficiently blocked. The superexchange interaction in **2**–**4** could be more thrivingly mediated through the Cu–Cl–Cu bridge if the magnetic orbitals had noticeable contribution from d_{z^2}. This, however, was not found in the Löwdin reduced orbital populations and the EPR spectra recorded for **2**–**4** revealed the $g_z >> g_x \approx g_y > 2.0023$ relation, which excludes significant d_{z^2} contribution to the magnetic orbitals**.**

As discussed above, the copper-carboxylato bridges in **5** lead to much stronger magnetic interaction and this is well reproduced in the DFT calculations (significantly negative *J* values). In general, the structure of the dimeric unit (Fig. 9) suggests two possible paths for the observed antiferromagnetic coupling, that is superexchange through the two carboxylato bridges and the δ overlap between the $d_{x^2-y^2}$-like SOMOs. The analysis of the respective orbitals exposed only one non-orthogonal magnetic pair with the spatial overlap S = 0.086 (Fig. 11), clearly indicating that the magnetic interaction in **5** is solely meditated through the two carboxylato bridges. This finding is in line with the previous study of Rodríguez-Fortea *et al*.[24c] It should be emphasized that accurate inclusion of electron correlation effects via DDCI2 and DDCI3 significantly improves the predictions, i.e. the triplet state is closer in energy to the singlet ground state. This demonstrates how important these effects are for an accurate estimation of magnetic coupling. The downside of the MRCI-type methods is their high and steeply rising computational cost. In this context, it seems important to notice that the combined B3LYP/DDCI3 approach has been demonstrated here to work well for the studied dinuclear system, allowing for recovery of at least a fraction of improvement that the DDCI3 calculations with a larger basis set could provide.

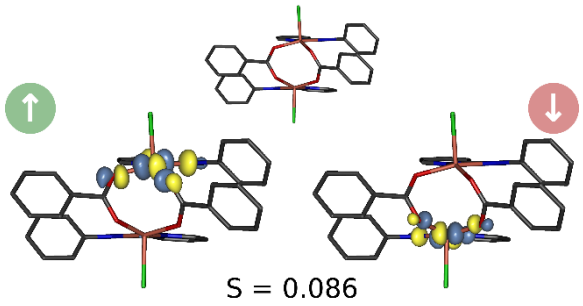

Figure 11. Pair of non-orthogonal magnetic orbitals of complex **5**.

The DFT calculations provided revealing insight into the role of three noncovalent interactions that can possibly mediate the exchange interaction in **1**. The *J* parameters in Table 4 demonstrate that these interactions route different types of

magnetic coupling in accordance with the literature data. The network of hydrogen bonds is predicted to introduce antiferromagnetic spin ordering (J < 0). The same type of magnetic coupling is transmitted by the π···π interaction, however the latter pathway is noticeably more efficient ($|J_{H\cdots O}| < |J_{\pi\cdots\pi}|$). On the other hand, the π···Cl interaction mediates ferromagnetic coupling between neighbouring Cu(II) ions. According to the DFT calculations the net value of J is slightly positive, for instance at the B97D/QVZPP it amounts to 0.14 cm^{-1}. This is very close to experimentally determined –2.3 cm^{-1}. The deviation between the theory and experiment of a few cm^{-1} at the DFT level is easily acceptable, but at the same time it shows that in the DFT calculations the role of H···O and π···π is underestimated, while the π···Cl interaction seems overestimated. All in all, the DFT calculations demonstrated that the value of J observed for **1** is a subtle interplay of three paths of magnetic exchange. Unfortunately, for such a large scale molecular models the application of multireference methods is a computationally prohibited task.

Conclusion

We explored coordination abilities of Schiff base ligands HL1, HL2 and HL3 derived from 2-pyridinecarbaldehyde and *o*-, *m*- and *p*-aminobenzoic acids, respectively, towards copper(II) chlorides in methanol and dmf. The results show that the position of the carboxylate group in the structural isomers HL1–HL3 influences the amount of chloride ligands in the coordination environments around copper atoms in **1**–**5**, which imposes the particular bridging pattern between metal centers. Combination of substituted benzoic acids and chloride ligands produced mono-, di- and polymeric complexes in which dimeric or polymeric structures are realized through bridging functions of solely chloride ligands (**2**–**4**) or carboxylate groups (**5**). The X-band polycrystalline EPR spectra of **1**–**4** confirm a square-pyramidal coordination geometry for these complexes suggested by the structural data. The EPR data show the absence of exchange interactions between copper ions in **1**–**4** in the range 295–77 K in accord with the experimental magnetic data and calculated exchange coupling constants. Complex **5** exhibited a characteristic spin-triplet EPR spectrum at 77 K that was simulated using the spin-Hamiltonian parameters for S = 1, g_x = 2.08, g_y = 2.11, g_z = 2.37 and the value of the zero-field splitting parameter D of 0.137 cm^{-1}. As expected, compounds **2**–**4** with copper-chloride bridges showed small coupling constants, while copper-carboxylato bridges in **5** lead to much stronger antiferromagnetic superexchange. The latter was well reproduced in the DFT, DDCI2 and DDCI3 calculations. For complexes **2**–**4** small values of exchange interactions but the sign of the J parameter (in the case of **2** and **3**) were predicted at the DFT theory level. Moreover, the DFT calculations demonstrated that in complex **1** the H···O and π···π interactions transmit antiferromagnetic coupling, while π···Cl brings about ferromagnetic coupling. Further theoretical work is needed for such calculations to reach a level at which they can guide the design of low-dimensional systems with specific magnetic lattices.

Experimental Section

Materials and Instrumentations

Commercially available chemicals were used as received; all experiments were carried out in air. Elemental analysis for Cu were performed by atomic absorption spectroscopy. Elemental analyses for CHN were performed using a Perkin-Elmer 2400 series analyzer. The IR spectra were recorded on a Perkin-Elmer 1600 FT–IR spectrometer (KBr pellet, 4000–400 cm^{-1}). Magnetic susceptibility measurements of powdered samples over the temperature range 1.8–400 K at the magnetic field of 5000 G and magnetization measurements at 2 K, between 0 and 50 000 G, were carried out with a SQUID magnetometer (Quantum Design MPMSXL-5). Corrections for the sample holders were applied. Diamagnetic corrections for the molecule were determined from Pascal's constants. X-band (9.8 GHz) EPR spectra were recorded on a Bruker ELEXSYS E500 instrument equipped with an NMR teslameter (ER 036TM) and a frequency counter (E 41 FC) and operating at microwave power of 10 mW, modulation amplitude of 0.5 mT and 2048 data points per spectrum. The experimental spectra were simulated using the program SPIN (S = 1/2, S > 1/2) written by Dr Andrew Ozarowski from NHMFL, University of Florida, with resonance field calculated by full diagonalization of energy matrix.

Synthesis

Syntheses of the Schiff base ligands

A methanol solution (10 ml) of 2-PCA (0.19 ml, 2 mmol) and the respective aminobenzoic acid (0.28 g, 2 mmol) in a 50 ml conic flask was heated to 50 °C and magnetically stirred for half an hour. The resultant yellow (HL1 and HL2) or brown (HL3) solution (with partially deposited Schiff base in the case of HL3 that was dissolved by adding 5 ml of DMF) was left in open air overnight and used as the ligand without further purification. HL2 was partially deposited overnight.

*Syntheses of $Cu(HL1)Cl_2{\cdot}CH_3OH$ (**1**) and $[Cu(L1)Cl]_2{\cdot}H_2O$ (**2**)*

To a stirred methanol solution of the ligand from the previous preparation (0.23 g, 1 mmol) $CuCl_2{\cdot}2H_2O$ (0.17 g, 1 mmol) dissolved in methanol (10 ml) was added. The solution that immediately turned blue-green, was heated to 50 °C and magnetically stirred for 20 minutes. The blue-green powder of **1** started to precipitate during the synthesis and was filtered off. Crystals suitable for crystallographic determination were formed by the next day. They were collected by filter-suction, washed with dry Pr^iOH and finally dried in air. Total yield: 66% (0.26 g). Elemental analysis calcd (%) for $C_{14}H_{14}Cl_2CuN_2O_3$ (392.71): C, 42.97; H, 3.58; N, 7.16; Cu, 16.11; found: C, 43.31; H, 3.62; N, 7.45, Cu 16.34%. Complex **2** was synthesized as described above by employing the crystalline copper salt and double amounts of the latter and HL1. Total yield: 72% (0.48 g). Elemental analysis calcd (%) for $C_{26}H_{20}Cl_2Cu_2N_4O_5$ (666.44): C, 46.85; H, 3.02; N, 8.40; Cu, 19.69; found: C, 46.76; H, 3.12; N, 8.48, Cu 19.50%.

*Syntheses of $[Cu(HL2)Cl_2]_2{\cdot}2DMF$ (**3**) and $[Cu(HL2)_2Cl]_nCl_n{\cdot}2nH_2O$ (**4**)*

To a flask with the light-yellow powder of HL2 in methanol from the previous preparation (0.45 g, 2 mmol) $CuCl_2{\cdot}2H_2O$ (0.34 g, 2 mmol) dissolved in DMF (10 ml) was added. The light-green solution was

heated to 50 °C and magnetically stirred until total dissolution of HL2 was observed (30 min). The resulting green solution was filtered and allowed to stand at room temperature. Green crystals of **3** suitable for crystallographic determination were formed within several days. They were collected by filter-suction, washed with dry Pr^{i}OH and finally dried in air. Yield: 71% (0.62 g). Elemental analysis calcd (%) for $C_{32}H_{34}Cl_4Cu_2N_6O_6$ (867.53): C, 44.30; H, 3.95; N, 9.68; Cu, 14.64; found: C, 44.48; H, 3.99; N, 9.84; Cu 14.77%. Complex **4** was synthesized as described above by employing the crystalline copper salt and a double amount of HL2. Yield: 68% (0.85 g). Elemental analysis calcd (%) for $C_{26}H_{24}Cl_2CuN_4O_6$ (622.93): C, 50.12; H, 3.98; N, 8.99; Cu, 10.20; found: C, 49.69; H, 3.91; N, 8.60; Cu 10.49%.

*Syntheses of [Cu(L3)Cl]$_n$ (**5**)*

To a stirred methanol/DMF solution of HL3 from the previous preparation (0.45 g, 2 mmol) crystalline $CuCl_2{\cdot}2H_2O$ (0.34 g, 2 mmol) was added. The solution that immediately turned dark-green was heated to 50 °C and magnetically stirred for 30 minutes. After that it was filtered and allowed to stand at room temperature. Green crystals of **5** suitable for crystallographic determination were formed within several days. They were collected by filter-suction, washed with dry Pr^{i}OH and finally dried in air. Yield: 75% (0.49 g). Elemental analysis calcd (%) for $C_{13}H_9ClCuN_2O_2$ (324.21): C, 48.15; H, 2.79; N, 8.64; Cu, 19.59; found: C, 48.36; H, 2.98; N, 8.39; Cu 19.47%.

Single crystal structure determination

Crystallographic data for the structures were collected at 100(2) K on an Oxford Diffraction Gemini (for **1, 2, 4** and **5**) or Xcalibur (for **3**) diffractometers using Mo-Kα (λ = 0.71073 Å) radiation or Cu-Kα (λ = 1.5407 Å) radiation in the case of **1** and **5**. Following analytical absorption corrections and solution by direct methods, the structures were refined against F^2 with full-matrix least-squares using the program SHELXL-97.[36] The hydroxyl hydrogen atoms in **1** were located and refined with O–H distances restrained to ideal values. Water molecule and OH hydrogen atoms in **2**, **3**, and **4** were refined with restrained O–H distances. Those for water molecule 2 of **4** could not be located. All remaining hydrogen atoms in **1**–**5** were added at calculated positions and refined by use of a riding model with isotropic displacement parameters based on those of the parent atom. Anisotropic displacement parameters were employed for the non-hydrogen atoms. Details of the data collection and processing, structure solution and refinement for **1**–**5** are summarized in Table 5.

Computational details

The ORCA 4.0.0 suite of programs was employed to perform DFT calculations.[37] To facilitate the comparison between theory and experiment, fragments of the X-ray structures were used as computational models after optimization of the positions of all hydrogen atoms (in the triplet state). This was accomplished with the GGA functional BP86,[38] which is known to provide accurate molecular structures,[39] and the def2-TZVP basis set.[40]

Table 6. Crystallographic data for **1**–**5**

	1	**2**	**3**	**4**	**5**
Empirical Formula	$C_{14}H_{14}Cl_2CuN_2O_3$	$C_{26}H_{20}Cl_2Cu_2N_4O_5$	$C_{32}H_{34}Cl_4Cu_2N_6O_6$	$C_{26}H_{24}Cl_2CuN_4O_6$	$C_{13}H_9ClCuN_2O_2$
Formula weight	392.71	666.44	867.53	622.93	324.21
Crystal system	Monoclinic	Triclinic	Triclinic	Monoclinic	Monoclinic
Space group	$P2_1/n$	$P\bar{1}$	$P\bar{1}$	$P2_1/n$	$C2/c$
T/K	100(2)	100(2)	100(2)	100(2)	100(2)
a/Å	10.9395(4)	7.0361(4)	8.7494(4)	13.4342(3)	17.953(3)
b/Å	7.2584(2)	12.7579(9)	10.0457(5)	7.59610(10)	8.6761(11)
c/Å	20.1320(6)	13.9481(9)	10.7161(4)	26.4071(4)	16.628(8)
α/°	90	79.443(6)	81.363(4)	90	90
β/°	104.764(3)	88.108(5)	81.972(3)	98.999(2)	116.78(2)
γ/°	90	80.272(6)	72.249(4)	90	90
Z	4	2	1	4	8
V/Å^3	1545.77(9)	1213.17(13)	882.45(7)	2661.61(8)	2312.2(12)
D_{cal}/g cm^{-3}	1.687	1.824	1.632	1.555	1.863
No. of reflections measured	12736	13309	18960	36411	5179
No. of independent reflections	2765	6109	5779	9553	2047
R_{int}	0.0556	0.0460	0.0333	0.0367	0.0825

Final R_1 values ($I>2\sigma(I)$)	0.0347	0.0595	0.0365	0.0436	0.0518
Final w$R(F^2)$ values ($I>2\sigma(I)$)	0.0844	0.1219	0.0867	0.0951	0.1246
Final R_1 values (all data)	0.0457	0.0859	0.0444	0.0594	0.0931
Final w$R(F^2)$ values (all data)	0.0910	0.1309	0.0905	0.1024	0.1511
CCDC No.	1572285	1572286	1572287	1572288	1572289

The optimization took advantage of the Split-RI-J approximation,[41] thus the appropriate auxiliary Coulomb fitting basis set was used.[42] At the DFT level the exchange coupling constants J ($H = \sum J_{ij} S_i S_j$) were theoretically predicted within the broken symmetry (BS) framework using the following formula:[43]

$$J = 2\frac{E_T - E_{BS}}{\langle S^2\rangle_T - \langle S^2\rangle_{BS}} \quad (4)$$

where E_T and E_{BS} are the energies of the triplet and broken symmetry state, respectively, and $\langle S^2\rangle_T$ and $\langle S^2\rangle_{BS}$ are the expectation values of the total square spin operator for the two states. In these calculations the hybrid B3LYP[44], hybrid meta-GGA TPSSh[45] and semiempirical GGA functional with a long-range dispersion correction B97D[46] were employed together with def2-SVP, def2-TZVP, def2-TZVPP and def2-QZVPP basis sets.[40] In the calculations with the functionals B3LYP and TPSSh the RIJCOSX approximation was used,[47] hence the appropriate auxiliary Coulomb fitting basis set was used.[42]

The exchange coupling for **5** was also determined by means of Difference Dedicated Configuration Interaction (DDCI2 and DDCI3),[48] as these methods are known to provide highly accurate values of J for molecular and extended magnetic systems.[49] In this case, the value of J was calculated as:

$$J = (E_S - E_T), \quad (5)$$

where E_S and E_T are the energies of the singlet and triplet state, respectively. The DDCI-type calculations were done with the minimal active space, CAS(2/2), where the two unpaired electrons occupy the two magnetic orbitals, i.e., the symmetric and antisymmetric combinations of the $d_{x^2-y^2}$-like orbitals. The molecular orbitals employed in the DDCI approach were computed using the Complete Active Space Self-Consistent Field (CASSCF) method for the triplet state. In these calculations the correlation-consistent basis sets cc-pVDZ was employed.[50] In addition, a combined approach similar to the ONIOM method was tested.[51] The exchange coupling parameter J was calculated as:

$$J = J(B3LYP/def2\text{-}QZVPP) + [J(DDCI/cc\text{-}pVDZ) - J(B3LYP/cc\text{-}pVDZ)] \quad (6)$$

Previously, this procedure has been proven successful, for instance in calculation of isotropic hyperfine coupling constants.[52]

Acknowledgements

All the computations were performed using computers of the Wrocław Centre for Networking and Supercomputing (Grant No. 47). MK and MW acknowledge financial support from a statutory activity subsidy from the Polish Ministry of Science and Higher Education for the Faculty of Chemistry of Wrocław University.

Keywords: 2-pyridinecarbaldehyde • *o*-, *m*- and *p*-aminobenzoic acids • Schiff base ligand • alpha-iminopyridine • Cu(II) chloride complexes• X-ray crystal structure • X-band EPR • magnetic measurements • DFT calculations

[1] V. Balzani, G. Bergamini, F. Marchioni, P. Ceroni, *Coord. Chem. Rev.* **2006**, *250*, 1254 – 1266.

[2] (a) S. Pasayat, M. Böhme, S. Dhaka, S. P. Dash, S. Majumder, M. R. Maurya, W. Plass, W. Kaminsky, R. Dinda, *Eur. J. Inorg. Chem.* **2016**, 1604 –1618; (b) B. C. Makhubela, A. M. Jardine, G. Westman, G. S. Smith, *Dalton Trans.* **2012**, *41*, 10715 – 10723.

[3] (a) S. Chen, R. Q. Fan, S. Gao, X. Wang, Y. L. Yang, *J. Luminesc.* **2014**, *149*, 75 – 85; (b) X. M. Wang, S. Chen, R. Q. Fan, F. Q. Zhang, Y. L. Yang, *Dalton Trans.* **2015**, *44*, 8107 – 8125.

[4] (a) B. Shaabani, A. A. Khandar, M. Dusek, M. Pojarova, F. Mahmoudi, *Inorg. Chim. Acta* **2013**, *394*, 563 – 568; (b) A. Hasheminasab, J. T. Engle, J. Bass, R. S. Herrick, C. J. Ziegler, *Eur. J. Inorg. Chem.* **2014**, 2643 – 2652.

[5] (a) S. Mukherjee, P. S. Mukherjee, *Crystal Growth & Design* **2014**, *14*, 4177 – 4186; (b) E. Lucaccini, M. Briganti, M. Perfetti, L. Vendier, J. P. Costes, F. Totti, R. Sessoli, L. Sorace, *Chem. Eur. J.* **2016**, *22*, 5552 – 5562.

[6] (a) A. Rotondo, G. Bruno, G. Brancatelli, F. Nicolò, D. Armentano, *Inorg. Chim. Acta* **2009**, *362*, 247 – 252; (b) R. H. Laye, E. C. Sañudo, *Inorg. Chim. Acta* **2009**, *362*, 2205 – 2212; (c) H. Yin, H. Liu, M. Hong, *J. Organomet. Chem.* **2012**, *713*, 11–19.

[7] (a) C. P. Landee, M. M.Turnbull, *Eur. J. Inorg. Chem.* **2013**, *13*, 2266 – 2285; (b) M. Grosshauser, P. Comba, J. Y. Kim, K. Ohto, P.Thuéry, Y. H. Lee, Y. Kim, J. Harrowfield, *Dalton Trans.* **2014**, *43*, 5662 – 5666; (c) S. N. Herringer, C. P. Landee, M. M. Turnbull, J. Ribas-Ariño, J. J. Novoa, M. Polson, J. L. Wikaira, *Inorg. Chem.* **2017**, *56*, 5441– 5454.

[8] (a) M. K. Singh, G. Rajaraman, *Chem. Eur. J.* **2015**, *21*, 980–983; (b) N. Van Well, M. Bolte, B. Delley, B. Wolf, M. Lang, J. Schefer, C. Rüegg, W. Assmus, C.Krellner, *Cryst.Eng.Comm.* **2017**, *19*, 1028 – 1034; (c) D. L. Reger, A. E. Pascui, E. A. Foley, M. D. Smith, J. Jezierska, A. Wojciechowska, S. A. Stoian, A. Ozarowski, *Inorg. Chem.* **2017**, *56*, 2884 – 2901.

[9] (a) E. A. Buvaylo, V. N. Kokozay, K. Rubini, O. Y. Vassilyeva, B. W. Skelton, *J. Mol. Struc.* **2014**, *1072*, 129 – 136; (b) E. A. Buvaylo, V. N. Kokozay, O. Y. Vassilyeva, B. W. Skelton, *Acta Cryst.* **2014**, E*70*, 164 – 166; (c) E. A. Buvaylo, V. N. Kokozay, O. Y. Vassilyeva, B. W. Skelton, *Acta Crystall. E* **2014**, *70*(4), 136 – 136; (d) E. A. Buvaylo, A. K. Melnyk, V. V. Trachevsky, O. Y. Vassilyeva, B. W. Skelton, *Polyhedron* **2016**, *105*, 238 – 245.

[10] (a) G. B. Deacon, R. J. Phillips, *Coord. Chem. Rev.* **1980**, *33*, 227 – 250; (b) K. Nakamoto, *Infrared and Raman Spectra of Inorganic and Coordination Compounds*, fifth ed., John Wiley, New York, 1997 (Part A and B).

[11] G. Murphy, P. Nagle, B. Murphy, B. Hathaway, *J. Chem. Soc., Dalton Trans.* 1997, 2645 – 2652.

[12] R. Mukherjee, *in Comprehensive Coordination Chemistry II*. From Biology to Nanotechnology, ed. J. A. McCleverty and T. J. Meyer, Elsevier **2004**, *6*, pp. 747 – 910.

[13] (a) S. K. Dey, B. Bag, K. M. Abdul Malik, M. S. El Fallah, J. Ribas, S. Mitra, *Inorg. Chem.* **2003**, *42*, 4029 – 4035; (b) A. Datta, D. K. Dey, W. S. Hwang, T. Matsushita, G. Rosair, *J. Chem. Research* **2005**, 502 – 504; (c) B. Bag, N. Mondal, S. Mitra, V. Gramlich, J. Ribas, M. S. El Fallah, *Polyhedron* **2001**, *20*, 2113 – 2116.

[14] (a) B. P. Buffin, E. B. Fonger, A. Kundu, *Inorg. Chim. Acta* **2003**, *355*, 340 – 346; (b) B. Bozic-Weber, E. C. Constable, C. E. Housecroft, M. Neuburger, J. R. Price, *Dalton Trans.* **2010**, *39*, 3585 – 3594; (c) C. M. Alvarez, R. Garcia-Rodriguez, D. Miguel, *J. Organomet. Chem.* **2007**,*692*, 5717 – 5726; (d) B. P. Buffin, P. J. Squattrito, A. O. Ojewole, *Inorg. Chem. Commun.* **2004**, *7*, 14 – 17; (e) D. Tzimopoulos, A. Czapik, M. Gdaniec, T. Bakas, A. A. Isab, A.-C. Varvogli, P. D. Akrivos, *J. Mol. Struct.* **2010**, *965*, 56 – 64.

[15] (a) B. K. S. Lundberg, *Acta Chem. Scand.* **1972**, *26*, 3977–3983; (b) W. A. Alves, I. O. Matos, P. M. Takahashi, E. L. Bastos, H. Martinho, J. G. Ferreira, C. C. Silva, R. H. de Almeida Santos, A. Paduan-Filho, A. M. Da Costa Ferreira, *Eur. J. Inorg. Chem.* **2009**, 2219 – 2228; (c) W. E. Estes, W. E. Hatfield, J. A. C. Van Ooijen, J. Reedijk, J. Chem. Soc., Dalton Trans. **1980**, 2121 – 2124; (d) M. Hernández-Molina, J. González-Platas, C. Ruiz-Pérez, F. Lloret, M. Julve, *Inorg. Chim. Acta* **1999**, *284*, 258 – 265; (e) G. A. van Albada, O. Roubeau, P. Gamez, H. Kooijman, A. L. Spek, J. Reedijk, *Inorg. Chim. Acta* **2004**, *357*, 4522 –4 527; (f) F. J. Barros-García, A. Bernalte-García, F. J. Higes-Rolando, F. Luna-Giles, A. M. Pizarro-Galán, E. Viñuelas- Zahínos, *Z. Anorg. Allg. Chem.* **2005**, *631*, 1898 – 1902; (g) X.-L. Li, B.-L. Liu, Y. Song, *Inorg. Chem. Commun.* **2008**, *11*, 1100 – 1102; (h) W. A. Alves, I. O. Matos, P. M. Takahashi, E. L. Bastos, H. Martinho, J. G. Ferreira, C. C. Silva, R. H. de Almeida Santos, A. Paduan-Filho, A. M. Da Costa Ferreira, *Eur. J. Inorg. Chem.* **2009**, 2219 – 2228.

[16] (a) T. Tadashi, W. Naofumi, N. Michio, M. Yoneichiro, M. Mitsuo, O. Shigeru, S. Yoshihiko, *Bull. Chem. Soc. Jpn.* **1990**, *63*, 364 – 369; (b) J. G. Rodriguez, M. Parra-Hake, G. Aguirre, F. Ortega, P. J. Walsh, *Polyhedron* **1999**, *18*, 3051 – 3055; (c) K. N. Lazarou, I. Chadjistamatis, A. Terzis, S. P. Perlepes, C. P. Raptopoulou, *Polyhedron* **2010**, *29*, 833 – 840; (d) G. S. Baghel, J. P. Chinta, A. Kaiba, P. Guionneau, C. P. Rao, *Cryst.Growth Des.* **2012**,*12*, 914 – 926; (e) J. Sundberg, H. Witt, L. Cameron, M. Hakansson, J. Bendix, C. J. McKenzie, *Inorg.Chem.* **2014**, *53*, 2873 – 2882.

[17] G. M. Brown, R. Chidambaram, *Acta Cryst.* **1973**, *B29*, 2393 – 2403.

[18] C. F. Jiang, F. P. Liang, Y. Li, X. J. Wang, Z. L. Chen, H. D. Bian, *J. Mol. Struct.* **2007**, *842*, 109 – 116.

[19] J. Hathaway, D. E. Billing, *Coord. Chem. Rev.* **1970**, *5*, 143 – 207.

[20] (a) R. P. Sharma, S. Kumar, P. Venugopalan, V. Ferretti, A. Tarushi, G. Psomas, M. Witwicki, *RSC Advances* **2016**, *6*, 88546 – 88558; (b) P. U. Maheswari, G. A. van Albada, B. Modec, B. Kozlevčar, J. Reedijk, *J. Mol. Struct.* **2012**, *1013*, 36 – 38; (c) A. K. Sharma, R. Mukherjee, *Inorg. Chim. Acta* **2008**, *361*, 2768 – 2776; (d) M. Barwiolek, E. Szlyk, A. Berg, A. Wojtczak, T. Muziol, J. Jezierska, *Dalton Trans*. **2014**, *43*, 9924 – 9933.

[21] G. A. Baker, G. S. Rushbrooke, H. E. Gilbert, *Phys. Rev*. **1964**, *135*, p. A1272.

[22] O. Kahn, *Molecular Magnetism*, Wiley-VCH, New York, 1993.

[23] E. I. Solomon, *Inorg. Chem.* **2006**, *45*, 8012 – 8025.

[24] (a) P. J. Hay, J. C. Thibeault, R. Hoffmann, *J. Am. Chem. Soc.* **1975**, *97*, 4884 – 4899; (b) S. Gehring, P. Fleischhauer, H. Padus, W. Haase, *Inorg. Chem.* **1993**, *32*, 54 – 60; (c) A. Rodríguez-Fortea, P. Alemany, S. Alvarez, E. Ruiz, *Chem. Eur. J.* **2001**, *7*, 627 – 637.

[25] (a) F. Neese, *Coord. Chem. Rev.* **2009**, *253*, 526 – 563; (b) C. Baffert, M. Orio, D. A. Pantazis, C. Duboc, A. G. Blackman, G. Blondin, F. Neese, A. Deronzier, M.-N. Collomb, *Inorg. Chem.* **2009**, *48*, 10281 – 10288; (c) M. Orio, D. A. Pantazis, T. Petrenko, F. Neese, *Inorg. Chem.* **2009**, *48*, 7251 – 7260; (d) S. K. Singh, N. K. Tibrewal, G. Rajaraman, *Dalton Trans.* **2011**, *40*, 10897 – 10906; (e) G. Rajaraman, F. Totti, A. Bencini, A. Caneschi, R. Sessoli, D. Gatteschi, *Dalton Trans.* **2009**, 3153 – 3161; (f) D. A. Pantazis, V. Krewald, M. Orio, F. Neese, *Dalton Trans.* **2010**, *39*, 4959 – 4967; (g) A. Tesmar, M. Witwicki, D. Wyrzykowski, A. Sikorski, D. Jacewicz, J. Drzeżdżon, L. Chmurzyński, *Polyhedron* **2017**, *127*, 144 – 152; (h) R. Modak, Y. Sikdar, A. Bieńko, M. Witwicki, M. Jerzykiewicz, S. Goswami, *Polyhedron* **2016**, *119*, 202 – 215. (i) M. C. Majee, T. Abtab, D. Mondal, M. Maity, M. Weselski, M. Witwicki, A. Bieńko, M. Antkowiak, G. Kamieniarz, M. Chaudhury, *Dalton Trans.*, **2018**, DOI: 10.1039/C7DT04389A (j) K. Muñoz-Becerra, D. Aravena, E. Ruiz, E. Spodine, N. Soto-Donoso, V. Paredes-García, D. Venegas-Yazigi, *Inorg. Chem. Front.*, **2017**, 4, 509-520.

[26] W. E. Marsh, K. C. Patel, W. E. Hatfield, D. J. Hodgson, *Inorg. Chem.* **1983**, *22*, 511 – 515.

[27] (a) D. D. Swank, G. F. Needham, R. D. Willet, *Inorg. Chem*. **1979**, *18*, 761–765; (b) W. E. Marsh, W. E. Hatfield, D. J. Hodgson, *Inorg. Chem*. **1982**, *21*, 2679–2684; (c) W. A. Alves, R. H. de Almeida Santos, A. Paduan-Filho, C. C. Becerra, A. C. Borin, A. M. D. C. Ferreira, *Inorg. Chim. Acta* **2004**, *357*, 2269–2278; (d) R. Li, B. Moubaraki, K. S. Murray, S. Brooker, *Dalton Trans*. **2008**, *43*, 6014–6022; (e) Y. Y. Kou, J. L. Tian, D. D. Li, H. Liu, W. Gu, S. P. Yan, *J. Coord. Chem*. **2009**, *62*, 2182–2192; (f) M. Mégnamisi-Bélombé, M. A. Novotny, *Inorg. Chem.* **1980**, *19*, 2470–2473; (g) S. Koohzad, H. Golchoubian, Z. Jagličić, *Inorg. Chim. Acta*. **2018**, *473*, 60–69; (h) F. Yraola, F. Albericio, M. Corbella, M. Royo, *Inorg. Chim. Acta*, **2008**, *361*, 2455–2461; (i) X.-H. Bu, M. Du, L. Zhang, Z.-L. Shang, R.-H. Zhang, M. Shionoya, *J. Chem. Soc., Dalton Trans.* **2001**, 729–735; (j) S. K. Hoffmann, D. K. Towle, W. A. Hatfield, K. Wieghardt, P. Chaudhuri, J. Weiss, *Mol. Cryst. Liq. Cryst*. **1984**, *107*, 161–170; (k) S.K. Hoffmann, D.K. Towle, W.A. Hatfield, P. Chaudhuri, K. Wieghardt, *Inorg. Chem*. **1985**, *24*, 1307–1312; (l) F. Tuna, L. Patron, Y. Journaux, M. Andruh, W. Plass, J.-C. Trombe, *J. Chem. Soc., Dalton Trans.* **1999**, 539–545; (m) C. J. O'Connor, *Inorg. Chim. Acta* **1987**, *127*, L29–L30; (n) X.-H. Bu, M. Du, Z.-L. Shang, L. Zhang, Q.-H. Zhao, R.-H. Zhang, M. Shionoya, *Eur. J. Inorg. Chem.* **2001**, 1551–1558; (o) J. N. Roedel, R. Bobka, B. Neumann, B. Weber, P. Mayer, I. P. Lorenz, *Z. Anorg. Allg. Chem.* **2007**, *633*, 1171–1177.

[28] (a) E. Kwiatkowski, M. Kwiatkowski, A. Olechnowicz, J. Mrozinski, D. M. Ho, E. Deutsch, *Inorg. Chim. Acta* **1989**, *158*, 37 – 42; (b) A. Bernalte-García, A. M. Lozano-Vila, F. Luna-Giles, R. Pedrero-Marín, *Polyhedron* **2006**, *25*, 1399 – 1407; (c) R. Singh, F. Lloret, R. Mukherjee, *Z. Anorg. Allg. Chem.* **2014**, *640*, 1086 – 1094; (d) M. Du, Y.-M. Guo, X.-H. Bu, J. Ribas, M. Monfort, *New J. Chem*. **2002**, *26*, 645 – 650; (e) T. Rojo, M. I. Arriortua, J. Ruiz, J. Darriet, G. Villeneuve, D. Beltran-Porter, *J. Chem. Soc., Dalton Trans.* **1987**, 285 – 291; (f) K. Skorda, T. C. Stamatatos, A. P. Vafiadis, A. T. Lithoxoidou, A. Terzis, S. P. Perlepes, J. Mrozinski, C. P. Raptopoulou, J. C. Plakatouras, E. G. Bakalbassis, *Inorg. Chim. Acta* **2005**, *358*, 565 – 582.

[29] (a) C. Desplanches, E. Ruiz, A. Rodríguez-Fortea, S. Alvarez, *J. Am. Chem. Soc.*, **2002**, *124*, 5197 – 5205; (b) S. H. Lapidus, J. L. Manson, H. Park, A. J. Clement, S. Ghannadzadeh, P. Goddard, T. Lancaster, J. S. Möller, S. J. Blundell, M. T. F. Telling, J. Kang, M.-H. Whangbo, J. A. Schlueter, *Chem. Commun*. **2013**, *49*, 499 – 501.

[30] A. M. Whyte, B. Roach, D. K. Henderson, P. A. Tasker, M. M. Matsushita, K. Awaga, F. J. White, P. Richardson, N. Robertson, *Inorg. Chem*. **2011**, *50*, 12867 –12876.

[31] (a) P. Gamez, *Inorg. Chem. Front*. **2014**, *1*, 35 − 43; (b) D. Bhattacharya, S. Shil, A. Misra, L. Bytautas, D. J. Klein, *J. Phys. Chem. A* **2016**, *120*, 9117 – 9130; (c) J. Martinez-Lillo, A. H. Pedersen, J. Faus, M. Julve, E. K. Brechin, *Cryst. Growth Des.* **2015**, *15*, 2598 – 2601.

[32] (a) W. E. Hatfield, *Comments, Inorg. Chem.* **1981**, *1*, 105 – 121; (b) C. P. Landee, R. Greeney, *Inorg. Chem.* **1986**, *25*, 3771 – 3775.

[33] A. Rodríguez-Fortea, P. Alemany, S. Alvarez, E. Ruiz, *Chem. Eur. J.* **2001**, *7*, 627 – 637 and refs therein.

[34] (a) D. L. Reger, A. Debreczeni, B. Reinecke, V. Rassolov, M. D. Smith, R. F. Semeniuc, *Inorg. Chem*. **2009**, *48*, 8911 – 8924; (b) W. Y. Gao,

R. Cai, T. Pham, K. A. Forrest, A. Hogan, P. Nugent, K. Williams, L. Wojtas, R. Luebke, Ł. J. Weseliński, M. J. Zaworotko, *Chem. Mater.* **2015**, *27*, 2144 – 2151; (c) N. R. de Campos, M. A. Ribeiro, W. X. Oliveira, D. O. Reis, H. O. Stumpf, A. C. Doriguetto, F. C. Machado, C. B. Pinheiro, F. Lloret, M. Julve, J. Cano, *Dalton Trans.* **2016**, *45*, 172 – 189.

[35] F. Neese, *J. Phys. Chem. Solids* **2004**, 65, 781 – 785.

[36] G. M. Sheldrick, *Acta Cryst*. **2008**, A*64*, 112 – 122.

[37] F. Neese, *Wiley Interdiscip. Rev. Comput. Mol. Sci.* **2012**, *2*, 73 – 78.

[38] (a) A. D. Becke, *Phys. Rev. A*, **1988**, *38*, 3098 – 3100; (b) J. P. Perdew, *Phys. Rev. B*, **1986**, *33*, 8822 – 8824.

[39] (a) F. Neese, W. Ames, G. Christian, M. Kampa, D. G. Liakos, D. A. Pantazis, M. Roemelt, P. Surawatanawong, S. Ye, *Adv. Inorg. Chem.* **2010**, *62*, 301– 349; (b) M. Witwicki, *Chem.Phys.Chem*. **2015**, *16*, 1912 –1925.

[40] F. Weigend, R. Ahlrichs, *Phys. Chem. Chem. Phys.* **2005**, *7*, 3297 – 3305.

[41] F. Neese, *J. Comput. Chem.* **2003**, *24*, 1740 – 1747.

[42] F. Weigend, *Phys. Chem. Chem. Phys*. **2006**, *8*, 1057 – 1065.

[43] (a) K. Yamaguchi, Y. Takahara, T. Fueno, in: V. H. Smith (Ed.), Applied Quantum Chemistry, Reidel, Dordrecht, **1986**, 155; (b) T. Soda, Y. Kitagawa, T. Onishi, Y. Takano, Y. Shigeta, H. Nagao, Y. Yoshioka, K. Yamaguchi, *Chem. Phys. Lett*. **2000**, *319*, 223 – 230.

[44] (a) A. D. Becke, *J. Chem. Phys*. **1993**, *98*, 5648 – 5652; (b) C. Lee, W. Yang, R. G. Parr, *Phys. Rev. B* **1988**, *37*, 785 – 789; (c) P. J. Stephens, F. J. Devlin, C. F. Chabalowski, M. J. Frisch, *J. Phys. Chem*. **1994**, *98*, 11623 – 11627.

[45] J. Tao, J. P. Perdew, V. N. Staroverov, G. E. Scuseria, *Phys. Rev. Lett*. **2003**, *91*, 146401 – 146405.

[46] S. Grimme, J. *Comput. Chem*. **2006**, *27*, 1787 – 1799.

[47] F. Neese, F. Wennmohs, A. Hansen, U. Becker, *Chem. Phys*. **2009**, *356*, 98 – 109.

[48] (a) R. Broer, W. J. A. Maaskant, *Chem. Phys*. **1986**, *102*, 103 – 111; (b) J. Miralles, O. Castell, R. Caballol, J.-P. Malrieu, *Chem. Phys*. **1993**, *172*, 33 – 43; (c) J. Miralles, J. P. Daudey, R. Caballol, Chem. Phys. Lett. **1992**, *198*, 555 – 562.

[49] (a) J. P. Malrieu, R. Caballol, C. J. Calzado, C. de Graaf, N. Guihery, *Chem. Rev*. **2014**, *114*, 429 – 492; (b) C. J. Calzado, J. F. Sanz, J.-P. Malrieu, *J. Chem. Phys*. **2000**, *112*, 5158 – 5167; (c) S. Vancoillie, J. Chalupský, U. Ryde, E. I. Solomon, K. Pierloot, F. Neese, L. Rulíšek, *J. Phys. Chem. B* **2010**, *114*, 7692 – 7702; (d) V. Barone, I. Cacelli, A. Ferretti, S. Monti, G. Prampolini, *J. Chem. Theory Comput*. **2011**, *7*, 699 – 706; (e) R. P. Sharma, A. Saini, P. Venugopalan, V. Ferretti, F. Spizzo, C. Angeli, C. J. Calzado, *New J. Chem*. **2014**, *38*, 574 – 583.

[50] (a) T. H. Dunning, Jr., *J. Chem. Phys*. **1989**, *90*, 1007 – 1023, (b) N. B. Balabanov, K. A. Peterson, *J. Chem. Phys*. **2005**, *123*, 64107 – 64107, (c) N. B. Balabanov, K. A. Peterson, J. Chem. Phys. **2006**, *125*, 74110 – 74120.

[51] S. Dapprich, I. Komáromi, K.S. Byun, K. Morokuma, M.J. Frisch, *J. Mol. Struct.(Theochem)*, **1999**, *1*, 461 – 462.

[52] (a) R. Improta, V. Barone, *Chem. Rev.* **2004**, *104*, 1231 – 1254. (b) M. Jerzykiewicz, I. Ćwieląg-Piasecka, M. Witwicki, A. Jezierski, *Chem. Phys.* **2011**, *383*, 27 – 34.

Entry for the Table of Contents

FULL PAPER

Five monomeric, dimeric and polymeric Cu(II) complexes with α-iminopyridine ligands have been used as platforms for detailed magnetostructural analysis of low-dimensional Cu(II) molecular magnetic systems. Theoretical methods supported magnetic-exchange pathways developed from the experimental data.

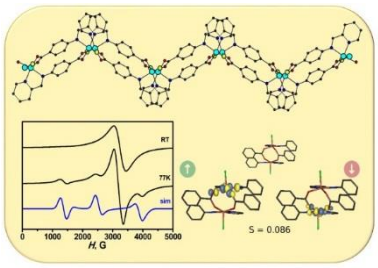

Magnetostructural correlations

*Elena A. Buvaylo, Vladimir N. Kokozay, Valeriya G. Makhankova, Andrii K. Melnyk, Maria Korabik, Maciej Witwicki, Brian W. Skelton, and Olga Yu. Vassilyeva**

Page No. – Page No.

Synthesis, Characterization, and Magnetic Properties of a Series of Copper(II) Chloride Complexes of Pyridyliminebenzoic Acids